Geochemistry Geophysics Geosystems G3

Article
Volume 12, Number 10
22 October 2011
Q0AE05, doi:10.1029/2011GC003704
ISSN: 1525-2027

Published by AGU and the Geochemical Society

Geochemistry of vent fluid particles formed during initial hydrothermal fluid–seawater mixing along the Mid-Atlantic Ridge

Verena Klevenz
Earth and Space Sciences Program, School of Engineering and Science, Jacobs University Bremen, Campus Ring 1, D-28759 Bremen, Germany (vklevenz@jacobs-alumni.de)

Wolfgang Bach
Fachbereich Geowissenschaften, Universität Bremen, D-28334 Bremen, Germany

Katja Schmidt
Earth and Space Sciences Program, School of Engineering and Science, Jacobs University Bremen, Campus Ring 1, D-28759 Bremen, Germany

Michael Hentscher
Fachbereich Geowissenschaften, Universität Bremen, D-28334 Bremen, Germany

Andrea Koschinsky
Earth and Space Sciences Program, School of Engineering and Science, Jacobs University Bremen, Campus Ring 1, D-28759 Bremen, Germany

Sven Petersen
Leibniz-Institut für Meereswissenschaften an der Universität Kiel (IFM-GEOMAR), D-24148 Kiel, Germany

[1] We present geochemical data of black smoker particulates filtered from hydrothermal fluids with seawater-dilutions ranging from 0–99%. Results indicate the dominance of sulphide minerals (Fe, Cu, and Zn sulphides) in all samples taken at different hydrothermal sites on the Mid-Atlantic Ridge. Pronounced differences in the geochemistry of the particles between Logatchev I and 5°S hydrothermal fields could be attributed to differences in fluid chemistry. Lower metal/sulphur ratios ($Me/H_2S < 1$) compared to Logatchev I result in a larger amount of particles precipitated per liter fluid and the occurrence of elemental sulphur at 5°S, while at Logatchev I Fe oxides occur in larger amounts. Systematic trends with dilution degree of the fluid include the precipitation of large amounts of Cu sulphides at a low dilution and a pronounced drop with increasing dilution. Moreover, Fe (sulphides or oxides) precipitation increases with dilution of the vent fluid by seawater. Geochemical reaction path modeling of hydrothermal fluid–seawater mixing and conductive cooling indicates that Cu sulphide formation at Logatchev I and 5°S mainly occurs at high temperatures and low dilution of the hydrothermal fluid by seawater. Iron precipitation is enhanced at higher fluid dilution, and the different amounts of minerals forming at 5°S and Logatchev I are thermodynamically controlled. Larger total amounts of minerals and larger amounts of sulphide precipitate during the mixing path when compared to the cooling path. Differences between model and field observations do occur and are attributable to closed system modeling, to kinetic influences and possibly to organic constituents of the hydrothermal fluids not accounted for by the model.

Copyright 2011 by the American Geophysical Union

Components: 13,400 words, 8 figures, 3 tables.

Keywords: Mid-Atlantic Ridge; geochemical modeling; geochemistry; hydrothermal fluids; hydrothermal mixing zone; particles.

Index Terms: 1009 Geochemistry: Geochemical modeling (3610, 8410); 1034 Geochemistry: Hydrothermal systems (0450, 3017, 3616, 4832, 8135, 8424).

Received 16 May 2011; **Revised** 8 September 2011; **Accepted** 13 September 2011; **Published** 22 October 2011.

Klevenz, V., W. Bach, K. Schmidt, M. Hentscher, A. Koschinsky, and S. Petersen (2011), Geochemistry of vent fluid particles formed during initial hydrothermal fluid–seawater mixing along the Mid-Atlantic Ridge, *Geochem. Geophys. Geosyst.*, *12*, Q0AE05, doi:10.1029/2011GC003704.

Theme: From the Mantle to the Ocean: Life, Energy, and Material Cycles at Slow Spreading Ridges
Guest Editors: C. Devey, N. Dublilier, J. Lin, N. Le Bris, and D. Connelly

1. Introduction

[2] The hydrothermal fluid – seawater mixing zone of deep-sea hydrothermal vents is the major habitat of the diverse hydrothermal vent fauna. It is characterized by the precipitation of large quantities of metal sulphide and oxide phases upon mixing of the hot, acidic, sulphide- and metal-enriched fluid with the cold, alkaline, oxygenated seawater. The particle-loaded fluid with the appearance of black smoke rises upwards in the water column, turbulently mixing with seawater, and forms the hydrothermal plume, which acts as the major dispersal mechanism for the heat and chemical fluxes of the hydrothermal vent [*Edmond et al.*, 1982; *Baker and Massoth*, 1986]. Iron oxyhydroxide particles staying in the non-buoyant hydrothermal plume act as important sink for dissolved elements in seawater [*German et al.*, 1991]. A major fraction of hydrothermal minerals however already settles down in close vicinity of the emanation site [*Feely et al.*, 1987], within the habitat of hydrothermal vent organisms like mussels, tubeworms, and shrimps. As a result hydrothermal minerals have been found within the guts of these animals and elevated metal concentrations have been found in their gills and digestion organs [*Zbinden et al.*, 2004; *Colaço et al.*, 2006; A. Koschinsky et al., Metal concentrations in the tissues of the hydrothermal vent mussel Bathymodiolus: Reflection of different metal sources, submitted to *Marine Environmental Research*, 2011]. Thus, since organisms appear to be influenced by the particulate metal load, one motivation to carry out this study on the geochemistry of particle formation in the hydrothermal mixing zone was to characterize the hydrothermal habitat. A comparison was done between mussel data (Koschinsky et al., submitted manuscript, 2011) and the respective particle chemistry of the same sites.

[3] The mineralogy and geochemistry of plume particles have been examined in numerous studies as far as the buoyant plume several meters above the emanation site and the non-buoyant plume or hydrothermal deposits are concerned [*Haymon and Kastner*, 1981; *Feely et al.*, 1987; *Dymond and Roth*, 1988; *Trocine and Trefry*, 1988; *Feely et al.*, 1990; *Mottl and McConachy*, 1990; *German et al.*, 1991; *Metz and Trefry*, 1993; *Feely et al.*, 1994, 1998; *Edmonds and German*, 2004]. The non-buoyant hydrothermal plumes mainly contain hydrous Fe oxides, with minor Fe, Cu, Zn sulphides. The major processes being responsible for the trace element geochemistry of the plume particles were identified as being co-precipitation from vent fluids, scavenging from seawater, and preferential settling from the plume and oxidative dissolution of Cu, Zn and Co bearing sulphide phases [*German et al.*, 1991]. In contrast, particles from the initial phase of mixing directly at the emanation site are much less studied. Black smoker particles were studied at vents on the Juan de Fuca Ridge by *Feely et al.* [1987], who reported sphalerite, wurtzite, pyrite, pyrrhotite, barite, chalcopyrite, cubanite, anhydrite, hydrous iron oxides, and elemental sulphur as main components. Sulphides are the dominant mineral phases in the black smoker particles. To our knowledge nothing has been published about particles precipitating from fluids diluted by less than 10% seawater, taken within the chimney. Analyzing particles from fluids at different dilutions as well as from nearly pure end-member fluids, allows comparing particle formation caused by mixing (which might subsequently be influenced by cooling) and

by conductive cooling. We therefore present results on the bulk geochemical composition of particles precipitated within hydrothermal fluid samples with seawater-dilutions ranging from 0–99%. The mineralogy was calculated from the chemical composition of the particle samples. Sample locations include basalt-hosted vent fields (Red Lion, Comfortless Cove, and Turtle Pits at 5°S on the Mid-Atlantic Ridge (MAR)) and an ultramafic-hosted vent field (Logatchev I at 15°N on the MAR).

[4] In order to distinguish between the mixing effect and the effect of pure cooling on particle formation at various vent sites with different fluid composition and temperatures, geochemical modeling using the geochemical software package Geochemist's Workbench® [*Bethke*, 2008] was performed. Differences between the observed mineralogy and geochemistry of precipitates and the theoretical equilibrium precipitation may help identifying additional processes influencing precipitation, e. g. organic ligands stabilizing metals in solution. *Sander and Koschinsky* [2011] showed by thermodynamic modeling that the presence of organic ligands significantly increases the dissolved metal concentrations in hydrothermal fluids.

2. Materials and Methods

2.1. Study Sites

[5] The Logatchev I hydrothermal field (14°45′N, 44°58′W) is located at about 3000 m water depth on a small plateau on the eastern flank of the inner rift valley of the MAR, south of the Fifteen-Twenty fracture zone [*Batuev et al.*, 1994]. It is situated in a tectonically controlled ultramafic setting. Besides the Rainbow field located at 36°N and the Nibelungen field at 8°18′S on the MAR, the Logatchev I field is one of the few active high-temperature (>300°C) fields influenced by the serpentinization of ultramafic rocks [*Douville et al.*, 2002; *Schmidt et al.*, 2007; *Melchert et al.*, 2008]. Extending ~800 m in NW-SE and >400 m in SW-NE direction, the Logatchev I field is characterized by a diversity of high- and low-temperature fluid emanations and faunal associations, including mussel beds of *Bathymodiolus puteoserpentis* and shrimp colonies of *Rimicaris* cf. *exoculatus* [*Petersen et al.*, 2009]. The mineralogy of the vent structures differs between the two venting styles occurring at Logatchev I, namely smoking craters (Quest, site B, Irina I, Candelabra, Anna Louise) and mound structures with chimneys (Irina II, Barad-Dur). The crater rims consist of the Cu sulphides chalcopyrite and isocubanite, as well as hematite, with only traces of pyrite, sphalerite, and anhydrite. In contrast, the mounds are built of sphalerite, pyrrhotite, with only minor chalcopyrite, whereas the smoker chimneys "Irina II microsmoker" and "Barad-Dur" are dominated by chalcopyrite, with rare magnetite and hematite [*Petersen et al.*, 2009].

[6] The measured and end-member composition of the fluids sampled at the different emanation sites within the Logatchev I hydrothermal field have been reported by *Charlou et al.* [2000], *Douville et al.* [2002], *Schmidt et al.* [2007], and *Schmidt et al.* [2011]. The fluids are characterized by high concentrations of dissolved H_2 and CH_4, as well as low concentrations of Si, Li, B and a low metal/H_2S ratio (≤1) in comparison to basalt-hosted systems, reflecting a hybrid alteration of both mafic and ultramafic host rocks. A uniform chemical composition and steady maximum temperature of ~350°C over more than 13 years indicate a stable system with continuous serpentinization in the sub-seafloor.

[7] In contrast to the ridge segment hosting the Logatchev I hydrothermal field, the 4°–9°S segment of the MAR is dominated by volcanic activity rather than by tectonics, as evidenced by young basaltic lavas indicating fresh or very recent volcanic activity at the active hydrothermal sites [*Haase et al.*, 2007]. The vent systems at 5°S comprises three active high temperature vent fields and several sites of diffuse emanations at depths of ~3000 m [*Haase et al.*, 2007; *German et al.*, 2008]. The chimney mineralogy consists of chalcopyrite – pyrite – sphalerite (Red Lion), chalcopyrite and pyrite (Sisters Peak), and pyrite – pyrrhotite – chalcopyrite – isocubanite (Turtle Pits). Sphalerite and massive blocks of anhydrite associated with magnetite and hematite form the mound surface at Turtle Pits [*Haase et al.*, 2007]. At the Turtle Pits field and at Comfortless Cove, 800 m northeast of Turtle Pits, boiling and phase separation of the fluid emanations is evident, with several smokers venting at or above the conditions of the critical point of seawater (407°C at 298 bar, which is the pressure at the seafloor at this site). The chemical composition of these fluid emanations is marked by a reduced chlorinity indicating the vapor phase of the phase-separated fluid, a major-element composition that is typical for basaltic systems and unusual high and highly variable trace-metal concentrations (Fe, Cu, Co, Mo) attributed to the high temperatures and specific properties of supercritical fluids [*Koschinsky et al.*, 2008]. The third vent field, Red Lion, lying ~2 km north of the Turtle Pits

field, displays maximum temperatures of 350°C and appears to be unaffected by phase separation. The chemical composition of its fluids is typical for basalt-hosted mid-ocean ridge systems, enriched in K, Ca, Na, Si and trace metals relative to seawater [*Koschinsky et al.*, 2008]. The most abundant animals at the high temperature vents were two shrimp species that colonized all active black smokers, with *Rimicaris* cf. *exoculata* dominating over *Mirocaris* sp. [*Haase et al.*, 2007].

2.2. Sample Collection and Analysis

[8] Samples of hydrothermal fluids were obtained from the vent fields Logatchev I I, Turtle Pits, Comfortless Cove, and Red Lion during seven research cruises between 2005 and 2009 with F/S Meteor (M64/2 in May 2005, M68/1 in May 2006, M78/2 in April 2009), F/S Maria S. Merian (MSM04/3 in Jan. 2007, MSM10/3 in Jan. 2009), and N/O Atalante (Ata1 in Dec./Jan. 2008/09, Ata2 in Jan. 2009), with ROV Quest (2005–2007) and ROV Kiel6000 (2008–2009). Samples were collected directly from inside vent orifices, either by means of an inert, Teflon® pumped flow-through system (Kiel Pumping System - KIPS: 9 bottles of 675 ml volume) mounted on the ROV [*Garbe-Schönberg et al.*, 2006], or with titanium syringe water samplers after *Von Damm et al.* [1985], manufactured by Brest Meca, France. The pure hot end-member fluid is clear and apparently free of particles, but blackens from a cloud of fine-grained sulphide particles precipitating as soon as it mixes with seawater at the vent orifice. Within this cloud, turbulent mixing is visible through the movement of the particles. It was possible to obtain a few samples with only ~1–2% seawater admixed, which were clear at the point of sampling. However, cooling over several hours until filtration on-board the research vessel caused precipitation of particles. Most of the samples are diluted by seawater by various degrees, since the turbulent mixing already starts within the chimney orifice. Samples only containing a very small proportion (<20%) of hydrothermal fluid were obtained at the fringe of the vent orifice or up to 20 cm above it.

[9] On-board, immediate measurements of pH, Eh, and H_2S were performed and fluid aliquots were taken after re-homogenization and filtered through 0.2 μM polycarbonate membrane filters (Nucleopore™). Filters were stored in a nitrogen-rinsed and sealed plastic container. It should be noted that the particles obtained this way represent both in situ precipitates which formed by mixing with seawater during or prior sampling as well as precipitates formed in the sample flasks upon cooling to ambient deep-sea temperature (it takes several hours after sampling until the ROV is taken on-board again, and fluid can be removed from the samplers). Further details on fluid sampling methods, sample treatment on board and temperature measurements are given by *Schmidt et al.* [2010, 2011].

[10] In the home lab, the filtered material was completely removed from the filter paper. In case of very fine material on the filter, the whole filter paper was digested together with the filtered material. For bulk geochemical analyses sample decomposition was performed in 30 ml PTFE vessels using a Picotrace DAS acid digestion system (Bovenden, Germany), with a mixture of 3 ml of 30% HCl, 1 ml of 65% HNO_3, and 1 ml of 40% HF at 180°C for 12 h. Following repeated acid evaporation and redissolution in 20% HCl, the digested samples were made up in a matrix of 0.5M HNO_3. Major and minor element concentrations (Mg, Al, S, Ca, Mn, Fe, Cu, Zn, Cd, Pb) were determined by ICP-OES (Spectro Ciros SOP CCD) and trace element concentrations (Co, Rb, Sr, Mo, Cs, Ba, W, U) were analyzed by ICP-MS using a collision-cell quadrupole (Perkin Elmer 500 DRCe) in the Jacobs University geochemistry lab. Accuracy and precision of the analytical method has been checked using the certified Fe-Mn oxide reference material JMn-1. For details on instrumental performance and the determination of method parameters such as method blanks, limit of quantification, precision and accuracy the reader is referred to *Alexander* [2008] and *Schmidt* [2010, chap. 6]. The calibration curve technique is used for both instruments, with calibration standards matching the sample acid matrix (for ICP-OES, calibration standards closely match the sample matrix with respect to elemental composition) and with internal standardization. The method precision of JMn-1 (i. e., precision of multiple sample decomposition and multiple analyses as % relative standard deviation) over a period of several years is better than 4% for all analyzed elements with ICP-OES and ICP-MS. The measured concentrations of JMn-1 are in very good agreement with published data, with less than 5% deviation from the average of published reference values (see GeoReM database). The accurate measurement of high sulphur concentrations has been ensured by using artificial spike solutions. Even though the particulate material available for geochemical analyses was very small in some cases, the measured concentrations were mostly well above the limit of quantification (ICP-MS) and

the limit of detection (ICP-OES). Blank filter material has been analyzed and its contribution to total elemental concentrations is less than 1% for Co, Rb, Sr, Cs, and U. Filter blank measurements with ICP-OES are below the detection limit for all elements determined. Results are reported as mass of particulate metal in the fluid. The major impact on the precision of reported particle concentration data derives from the uncertainty of the filtered fluid volume, which has sometimes just been estimated and may vary by about 10%.

[11] Compositional data of the hydrothermal fluid samples used for this study are partly reported in previous publications [*Schmidt et al.*, 2010, 2011] or were obtained during this study and were used for the calculation of partition coefficients. Analytical details and information about reference materials, precision and accuracy are given by *Schmidt et al.* [2011].

[12] The mineralogy and mineral chemistry of selected particle samples from 5°S vent fields was analyzed by investigating small subsamples that were mounted on aluminum stubs using carbon tapes, coated with Au–Pd and investigated with a JEOL JXA 8200 Superprobe using backscatter and secondary electron images as well as energy-dispersive microprobe analysis (EDX; V = 15 kV, I = 20 nA, beam diameter of 2 μm) at IFM-Geomar in Kiel.

2.3. Thermodynamic Calculations

[13] Particle precipitation was modeled for the fluids of Logatchev I, Red Lion, Comfortless Cove and Turtle Pits along two different reaction paths to calculate the effects of cooling and mixing with seawater. The different paths were chosen to assess the range of processes involved in particle formation. Particles retrieved from vent fluid samplers may have formed within the sampler or they may represent plume particles, which were entrained inadvertently when the vent fluid was collected. Which of the two types dominates is largely constrained by the amount of seawater entrainment upon sampling. If very little seawater is admixed to the vent fluid sample (high-quality sample with low Mg contents), most of the particles have formed within the sampler upon conductive cooling. If the nozzle of the sampler is not placed well within the vent orifice, seawater entrainment and particle formation prior to fluid sampling takes place. This process is believed to contribute most of the particles in samples with large fractions of seawater (i.e., high Mg contents).

[14] We conducted thermodynamic calculations to predict which minerals should form due to (1) conductive cooling after admixing a small fraction of seawater (cooling model), and (2) mixing with large fractions of seawater and cooling entirely related to mixing (mixing model). In the cooling model, the fluid was first mixed with 3% seawater to produce a typical high quality fluid sample retrieved from the vent orifice (based on low Mg concentrations, the proportions of seawater entrained during sampling are less than a few percent). Minerals precipitated during the mixing step were added to the minerals precipitated during the cooling step, as it can be assumed, that particles formed during initial mixing are also collected together with the fluid. The cooling path predicts the amount of minerals formed by closed-system cooling in the sample bottle after sampling. In the mixing model, the end-member hydrothermal vent fluids were mixed with 2°C seawater to a final temperature of 25°C to predict mineral precipitation during turbulent mixing in the buoyant plume.

[15] In both types of model calculations, it was assumed that the minerals form instantaneously in equilibrium with the solution; however, re-equilibration of minerals and solution upon cooling was suppressed. This strategy enables us to track the rapid formation of "black smoke" while preventing spontaneous equilibration at low temperature where reaction rates are slow relative to the time scales of sample retrieval (hours).

[16] All models were re-run with the precipitation of all minerals suppressed to calculate the saturation state of minerals. These calculations become relevant, when thermodynamic predictions of stable phase relations and observations do not match and metastable states need to be assessed.

[17] The React module of the Geochemist's Work Bench (GWB) was employed to perform the calculations [*Bethke*, 1996]. End-member fluid compositions used in the calculations are provided in Table 1. To cover the temperature range up to 400°C of high-temperature vent fluids, a Log K database for GWB was created, which is valid for temperatures between 0 and 400°C at constant pressure of 500 bars. SUPCRT92 [*Johnson et al.*, 1992] with the OBIGT database [*Dick*, 2008] was used to calculate equilibrium constants, which were then compiled in the tailored GWB database. The thermodynamic data used for aqueous species of Fe and Cu are as in the work by *Tivey et al.* [1995]. An extended Debye–Hückel equation [*Helgeson*, 1969]

Table 1. Model Input Parameter: Fluid End-Member Compositions [*Schmidt et al.*, 2007; *Koschinsky et al.*, 2008]

	Unit	Logatchev I	Red Lion	Sisters Peak	Turtle Pits	Seawater
Temperature	°C	350	349	400	400	4
pH (25°C)		3.3	3.5	3.1	3.1	7.8
Mg++	molal	0	0	0	0	53
Methane	μmolal	3500	60	6	30	0
H2S	mmolal	2.5	6	9	5	0
H2	mmolal	19	0.4	0.4	0.6	0
O2	mmolal	0	0	0	0	0.2
SO4−	mmolal	0	0	0	0	29.5
Cl^-	mmolal	551	552	224	271	560
Br-	μmolal	837	873	392	482	838
CO2	mmolal	10.1	10	6.7	13	2.4
B(OH)3	μmolal	335	520	591	547	450
SiO2	mmolal	8.6	21.8	14.4	11.6	0.036
Na^+	mmolal	455	480	209	237	480
K+	mmolal	24	19.8	7.4	8.6	9.8
Ca++	mmolal	29	18.6	17.4	8.8	10.2
Li+	μmolal	252	1217	343	427	26
Fe++	μmolal	2410	803	3380	3940	0.0045
Mn++	μmolal	338	730	704	473	0.0013
Cu+	μmolal	44	5.2	102	76	0.0033
Zn++	μmolal	36	60	155	69	0.028
Co++	μmolal	0.75	0.4	1.1	0.88	1.50E-05
Pb++	μmolal	0.138	0.182	0.21	0.184	1.30E-05

was used to calculate activity coefficients with B–dot extended parameters and hard core diameters for aqueous species from *Wolery* [2004]. Dissolved neutral species were assigned an activity coefficient of one, except non–polar species for which CO_2 activity coefficients were used [*Drummond*, 1981]. Kinetically sluggish redox reactions involving sulfur species were suppressed by decoupling sulfide and sulfate. Likewise, the reaction between H_2(aq) and O_2(aq) was also suppressed. Other redox reactions (e.g., the oxidation of Fe^{2+} to Fe^{3+}) were allowed. Mineral compositions used in the calculations are idealized; no substitutions or solid solutions were taken into account.

3. Results and Discussion

3.1. Geochemistry of Vent Particles in Comparison to Fluid Chemistry

[18] The results of bulk analyses of filtered particles are given as moles per volume and are presented in Table 2. The data provide a measure of the total mass of particulate metal in the fluid. Also, when combined with fluid compositional data, the bulk particle analyses yield information about the partitioning of a metal between the fluid and the particles.

3.1.1. Sulphur and Major Sulphide Forming Metals (Fe, Cu, Zn)

[19] The bulk elemental composition of the particles is marked by a dominance of S in all samples. Sulphur concentrations range from 20 to 520 μM with one maximum value of 913 μM in the Logatchev I samples and from 200 to 1800 μM in 5°S samples (Table 2). Significantly lower S concentrations in Logatchev I samples than in 5°S samples are consistent with the fluid-chemistry at these sites. Comparing the S concentrations of the particles to fluid end-member H_2S concentrations reveals that only about 2–17% of the H_2S content is precipitated in sulphide minerals, while the rest probably undergoes oxidation [*Mottl and McConachy*, 1990] and uptake by organisms [e.g., *Johnson et al.*, 1988].

[20] A good positive correlation between S and Fe concentration (R^2 = 0.67 for Logatchev I samples, R^2 = 0.74 for 5°S samples), as well as slight to moderate positive correlations between S and Cu (R^2 = 0.62 for Log. samples, R^2 = 0.23 for 5°S samples), and S and Zn (R^2 = 0.12 for Log. samples, R^2 = 0.28 for 5°S samples) indicates that sulphides are the main components of the particles (Figure 1). Similar to S, also the sulphide-forming

Table 2. Geochemical Data of Particles From 5°S Hydrothermal Fields and Logatchev I Venting Sites[a]

Vent	Sample	Fluid (%)	T Max[b] (°C)	pH (25°C)	S (μM)	Fe (μM)	Zn (μM)	Cu (μM)	Ca (μM)	Mg (μM)	Al (μM)	Mn (nM)	Co (nM)	Pb (nM)	Cd (nM)	Sr (nM)	Mo (nM)	Ba (nM)	Rb (nM)	Cs (nM)	W (nM)	U (nM)	Me[c]/S
									5°S														
Sisters Peak	M68/1 20ROV5	32	350	3.2	1072	234	46.4	112	223	11.9	2.9	224	254	64	110	692	128	18	3.9	3.1	–	0.14	0.37
	M68/1 20ROV6	87	380	3.1	353	82	25.4	62.1	1.4	1.4	1.0	–	228	66	44	10	76	–	0.6	0.32	0.14	0.10	0.48
	Ata 42ROV2−5,7	~70	367	~4.5	713	91	60.2	43.7	1.8	2.9	0.50	–	55	–	91	8	51	4.7	0.4	0.26	0.20	0.03	0.27
	Ata 42ROV11+12	~20	n. d.	~6	1472	391	56.2	11.6	6.6	23.7	4.6	434	36	–	128	77	53	–	2.1	3.7	0.11	0.13	0.31
	Ata 42ROV14	8	n. d.	6	738	145	6.7	2.1	6.0	31.7	1.1	–	18	17	–	57	12	12	1.2	0.16	0.15	0.22	0.21
	M78/2 308ROV8	32	375	4.2	n.d.	108	2.7	13.4	2.6	25.9	38	287	52	22	–	38	30	–	3.6	0.30	–	0.07	
	M78/2 308ROV7	79	375	2.4	n.d.	366	114	139	8.0	9.7	2.7	951	520	953	228	37	43	–	3.3	0.10	0.15	0.03	
	M78/2 308ROV6	64	375	2.7	n.d.	208	76.0	12.4	10.1	16.9	9.8	724	289	200	–	49	29	–	–	1.3	–	0.04	
	M78/2 308ROV5	55	375	3.8	n.d.	142	51.1	6.8	10.7	40.1	4.6	724	243	142	–	74	45	–	6.4	0.48	–	0.05	
Turtle Pits	M68/1 3ROV10	88	395	3.2	212	50	16.2	42.7	2.3	22.1	2.6	237	322	49	28	6	45	1.2	0.8	0.42	–	0.07	0.52
	M68/1 12ROV5	76	405	3.4	295	44	45.3	14.2	4.3	12.2	0.86	–	340	115	59	25	37	2.5	2.6	0.07	0.05	0.20	0.35
	M68/1 12ROV8	95	407	3.1	250	33	37.4	17.9	8.3	18.4	6.0	–	293	81	33	27	27	6.1	2.1	0.32	0.08	–	0.35
	Ata 35 ROV8	99.7	429	2.9	217	122	29.9	53.8	4.6	1.8	1.2	–	261	61	–	15	47	4.0	2.1	0.09	0.40	0.59	0.95
	Ata 46ROV7	42	412	3.5	1576	892	27.4	60.1	197	28.9	5.7	–	273	77	120	292	107	5.8	0.8	0.07	0.17	1.53	0.62
	Ata 57ROV2,3,5	~30	371	~5	661	162	7.7	17.7	3.4	8.6	0.79	–	227	33	–	48	37	1.7	0.7	0.90	0.34	0.24	0.28
	Ata 57ROV4	79	371	2.9	1401	294	32.0	92.0	11.6	14.7	0.89	–	916	126	–	51	82	7.3	5.2	0.52	0.15	0.35	0.30
	M78/2 281ROV1	94	425	2.6	n.d.	97	26.3	57.1	3.0	1.6	0.91	278	224	64	–	–	31	–	1.7	0.03	0.10	–	
	M78/2 281ROV2	100	425	2.4	n.d.	74	36.4	71.6	12.7	3.1	14	773	330	117	–	41	67	–	8.1	1.8	0.43	–	
Red Lion	Ata 67ROV5−7	~70	363	~4	1796	702	166.4	108	29.7	3.3	3.8	1421	29	120	391	119	35	18	3.0	0.60	0.10	0.04	0.54
	Ata 67ROV4+7	~55	363	~4.5	672	86	58.8	3.5	4.9	10.7	0.75	209	8		99	34	29	–	2.3	0.56	–	0.06	0.22
	M78/2 297ROV6	80	348	3.8	n.d.	85	21.7	5.2	6.1	5.1	0.87	392	57	195	–	28	18	–	5.9	0.07	–	0.01	
									Logatchev I														
Baradur	Ata 13ROV 1	1.3	365	7.6	37	52	0.8	19.7	4.9	24.9	0.99	344	42	3	16	50	–	10			–	1.07	1.96
	MSM04/3 275ROV5	99	n. d.	n. d.	96	35	28.6	36.3	2.7	–	0.59	–	246	106	n. d.	13	–	55	2.3	0.05	2.18	0.01	1.04
Site B	Ata 30ROV5	93	n. d.	3.5	109	37	12.8	25.1	3.7	0.5	0.25	–	550	98	18	35	–	72	5.6	0.81	0.45	1.01	0.69
	Ata 30ROV3	90	352	3.9	160	70	11.3	38.6	11.3	1.8	0.56	–	581	51	–	69	9	132	13	0.22	0.25	0.06	0.75
	Ata17ROV3	90	363	3.8	50	20	18.0	3.7	7.7	1.8	0.20	–	211	43	–	39	–	19	8.1	0.14	0.11	0.02	0.82
	MSM10/3 313ROV12	87	350	4	162	36	25.8	7.3	7.8	2.8	0.62	127	345	61	29	45	8	14	9.7	0.76	0.23	0.03	0.43
	MSM04/3 255ROV4	98	n. d.	3.6	125	52	22.8	40.3	8.0	2.0	0.35	–	330	99	n. d.	37	–	55	7.2	0.18	0.50	1.98	0.92
	MSM04/3 255ROV3	98	343	4.2	80	35	21.2	27.2	1.3	–	0.03	–	159	93	n. d.	8	9	38	1.3	0.18	0.12	0.33	1.04
Candelabra	Ata30ROV8	90	362	4.2	57	31	6.4	24.3	9.0	2.0	0.25	–	324	39	–	63	10	82	10.6	0.45	1.37	0.05	1.09
	MSM04/3 255ROV17	98	335	4.2	97	42	29.2	30.8	5.2	–	0.52	–	264	294	n. d.	27	–	97	5.2	0.46	0.31	0.01	1.06
Quest smoker	Ata 24ROV11	45	n. d.	5.7	146	17	7.9	9.8	4.3	9.6	0.51	–	200	42	–	50	30	–	–	–	–	–	0.24
	MSM04/3 259ROV25	99	347	3.5	113	26	20.9	26.5	2.4	0.4	0.48	–	221	60	n. d.	11	–	7	2.2	0.08	0.97	0.02	0.65
Irina II microsmoker	Ata 24ROV2	94	362	3.5	44	11	17.0	3.6	8.3	1.0	0.21	–	40	28	–	50	–	–	–	–	–	–	0.73
	Ata 24ROV5	8	364	6.6	75	148	2.6	3.1	7.2	16.7	1.3	–	70	–	24	100	–	–	–	–	–	–	2.06
	MSM10/3 290ROV11	80	352	3.8	279	92	14.1	17.7	17.8	5.4	0.18	202	165	29	27	129	11	261	10.3	0.48	0.20	0.11	0.44
	MSM04/3 244ROV7	99	n. d.	4.0	111	46	27.2	33.3	5.9	–	0.36	–	190	450	n. d.	34	11	166	5.7	0.19	0.31	0.00	0.95

Table 2. (continued)

Vent	Sample	Fluid (%)	T Max[b] (°C)	pH (25°C)	S (μM)	Fe (μM)	Zn (μM)	Cu (μM)	Ca (μM)	Mg (μM)	Al (μM)	Mn (nM)	Co (nM)	Pb (nM)	Cd (nM)	Sr (nM)	Mo (nM)	Ba (nM)	Rb (nM)	Cs (nM)	W (nM)	U (nM)	Me[c]/S
	MSM04/3 253ROV9	98	n. d.	4.0	192	76	40.2	42.8	6.2	–	0.24	–	629	285	n. d.	29	11	12	6.1	0.21	0.57	–	0.83
Irina II, main structure	MSM04/3 244ROV3	64	293	n. d.	913	470	14.6	104	3.1	3.6	0.68	–	171	31	n. d.	35	99	189	7.4	10.90	0.05	0.11	0.64
Irina I smoker	Ata17ROV13	23	370	5.9	20	15	1.3	1.2	1.4	3.9	0.54	–	92	17	–	36	17	22	3.6	2.97	0.26	0.06	0.86
	MSM04/3 255ROV12	47	n. d.	5.2	311	150	13.6	23.8	3.1	4.0	4.8	–	342	69	n. d.	40	20	277	2.4	0.84	0.26	0.27	0.60
Anna Louise smoker	Ata 13ROV10	43	352	5.43	226	176	12.1	15.9	10.4	17.0	1.8	–	374	43	–	73	54	30	12.7	22.05	0.66	0.24	0.90
	Ata 13ROV9	11	352	8.3	49	12	2.2	1.6	3.6	14.7	1.8	–	37	8	–	33	–	6	1.7	0.74	0.12	0.13	0.32
	Ata 13ROV6	10	353	6.6	26	12	1.3	0.5	1.9	10.0	3.1	–	11	10	–	37	–	17	1.7	0.90	–	0.14	0.54
	MSM10/3 315ROV19	78	330	4.4	519	237	24.3	41.5	3.8	3.5	0.38	310	576	81	74	30	18	19	6.8	0.55	0.44	0.07	0.58
	MSM04/3 275ROV7	98	n. d.	4.2	103	42	28.3	34.9	3.6	–	0.99	–	232	94	n. d.	17	10	14	3.4	0.24	–	0.01	1.02
Mixed sample	Ata 30ROVA1	12	n. d.	n. d.	47	281	1.1	3.2	9.4	21.0	1.8	155	41	7	29	147	–	130	3.2	0.09	0.15	1.23	6.05

[a]Concentrations are given in moles/kg hydrothermal fluid. Fluid% gives the proportion of endsmember fluid in the hydrothermal fluid – seawater mixture from which the particle sample is derived. A dash is used if the concentration was below detection limit, 'n. d.' means not determined.
[b]T max refers to the maximum temperature measured in the vent orifice during the duration of one sampling procedure; it does not give the exact temperature of the respective sample.
[c]Me stands for the sum of Fe + Zn + Cu.

metals Fe, Cu and Zn precipitate in larger amounts from the 5°S fluids than from the Logatchev I fluids, which is related to slightly higher concentrations of these metals in the fluids of 5°S (Turtle Pits and Comfortless Cove) compared to the Logatchev I fluids, and to the higher H_2S concentrations in the fluids of 5°S. The lower Fe/H_2S ratio in the fluids at 5°S, compared to the Logatchev I fluids results in a higher potential for metal-sulphide precipitation at 5°S than at Logatchev I.

[21] The amount of Fe precipitating is not correlated with the Fe concentration in the vent fluids, while there is a good correlation of Cu and Zn particle concentrations with non-filtered (total) fluid concentrations (Figure 2). The reason for this is that the total Cu and Zn fluid concentration is dominated by the particulate phase already at low mixing ratios of vent fluid with seawater. In contrast, only a small fraction of the total Fe content of the fluid is precipitated (mostly <10%, *Schmidt et al.* [2011] compare fluid composition of filtered and non-filtered samples from the Logatchev I vent field). Moreover, the fraction of Fe precipitating increases with fluid dilution by seawater (Figure 3), which is counteracting a positive correlation between particle and fluid concentration. Resulting particle-bound Fe amounts are similarly large at low and high Fe fluid concentrations, preventing any correlation between fluid and particulate Fe concentrations.

[22] Figure 5 shows the fractions of all metals in the precipitates relative to their respective concentration in the non-filtered fluid samples. Cadmium, Cu, Zn, Co, Pb, and Mo are the elements displaying $Me_{particle}/Me_{fluid}$ ratios clustering around 1. Tungsten, Fe, and U show a large variability of the $Me_{particle}/Me_{fluid}$ ratio in the intermediate range from 0.007–0.7, while Cs and Ba show a similar ratio but at lower levels ranging from 0.0001–0.01. Strontium, Rb, Mg, Mn, and Ca have the lowest $Me_{particle}/Me_{fluid}$ rations and range between 0.00005 and 0.006. Samples with anhydrite as a major phase in the particles differ from this trend (M68/1 20ROV5, Sisters Peak (Comfortless Cove), and Ata2 46ROV7, Turtle Pits, both 5°S), and show higher fractions of Ca and Sr partitioned into the particles with $Me_{particle}/Me_{fluid}$ ratios of about 0.01.

[23] Some samples show $Me_{particle}/Me_{fluid}$ ratios >1 for Cu and/or Zn (Figure 2) or for the sulphide-forming trace metals Co, Pb, Mo, Cd (Figure 4) implying that the amount of metal precipitated as particles is larger than its concentration in the

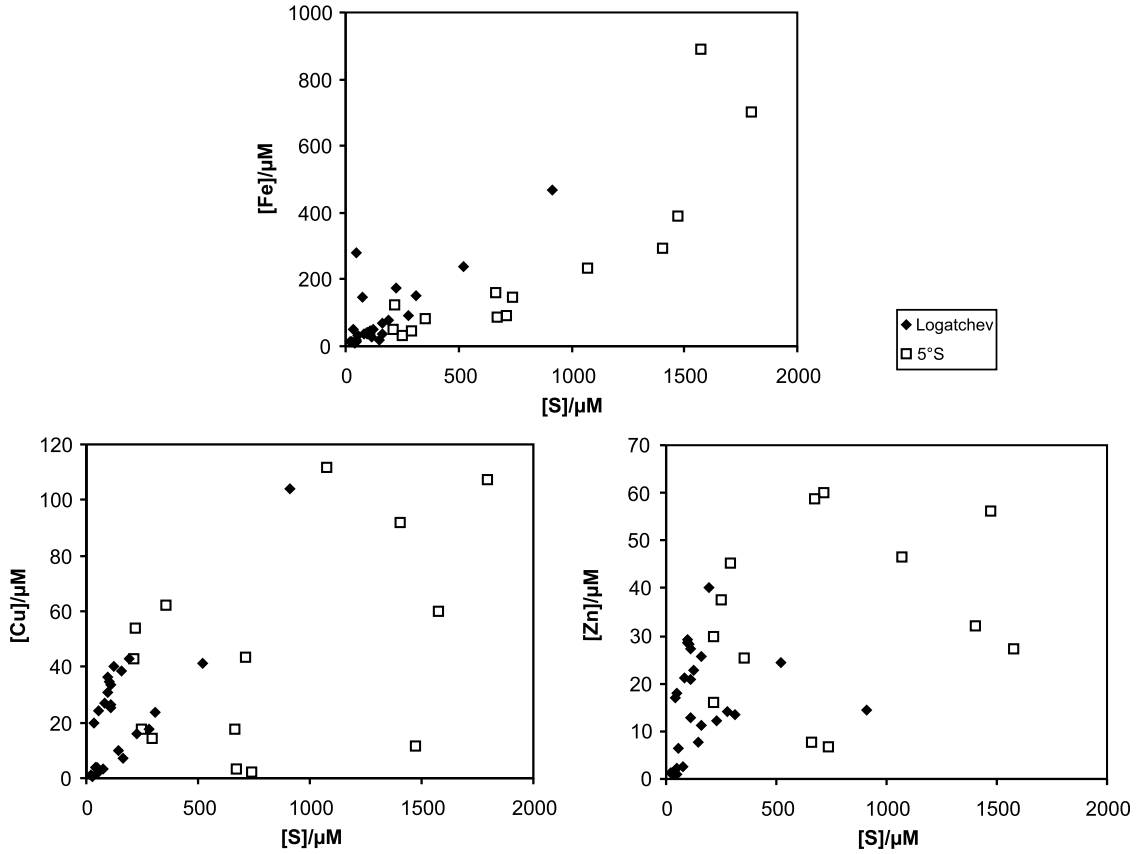

Figure 1. Correlation of Fe, Cu and Zn with S concentrations in the particles of Logatchev I and 5°S vents.

original fluid. This can be explained by heterogeneous partitioning of particles between filtered and un-filtered aliquots. As there could be either more particles in the un-filtered or in the filtered aliquot, some fractions of metal precipitated would occur too high, while others would be estimated too low, therefore the observed range of fractions precipitated is larger than in reality.

3.1.2. Trace Metals (Co, Mo, Pb, Cd, Mn, U)

[24] Among the trace metals, Co has the highest concentration in all particle samples of Logatchev I and 5°S, commonly ranging from 10 nM to 600 nM for both areas. At Turtle Pits there is one sample with 900 nM. The particles' Co content tends to be high at high Cu concentrations, confirming an affinity of Co for chalcopyrite [*Hannington et al.*, 1991; *Metz and Trefry*, 2000; *Schmidt et al.*, 2007]. The same is true for Mo, also known to precipitate with high temperature Cu-sulphides [*Fouquet et al.*, 1988; *Hannington et al.*, 1991; *Tivey et al.*, 1995]. A covariance of Cu, Co, and Mo was also observed in the fluids of Turtle Pits and Sisters Peak, which suggests a similar control on their mobility [*Koschinsky et al.*, 2008]. The solubility of Cu, Co, Mo is known to be strongly temperature-controlled due to the sharply decreasing solubility of chalcopyrite between 400 and 300°C [*Seyfried and Ding*, 1995]. The amounts of Co and Mo precipitated from the fluids both show a positive correlation with their respective calculated end-member fluid concentration in non-filtered aliquots, because >99% of the total metal content belongs to the particulate fraction. There is, however, a major difference in the Mo content of the smoke particles between Logatchev I and 5°S, with higher concentrations in 5°S particles (average 50 nM) and lower in Logatchev I (mostly between 8 and 20 nM, or often below detection limit). This might be related to higher fluid concentrations of Mo at 5°S (end-member concentrations of 32–62 nM at Turtle Pits (K. Schmidt, unpublished data, 2006, 2008; V. Klevenz, unpublished data, 2009)) compared to those at Logatchev I (calculated end-member concentrations of 0–6 nM [*Schmidt et al.*, 2011]) which can likely be attributed to the very high fluid temperature during venting at Turtle Pits (~400°C), increasing the solubility of Mo

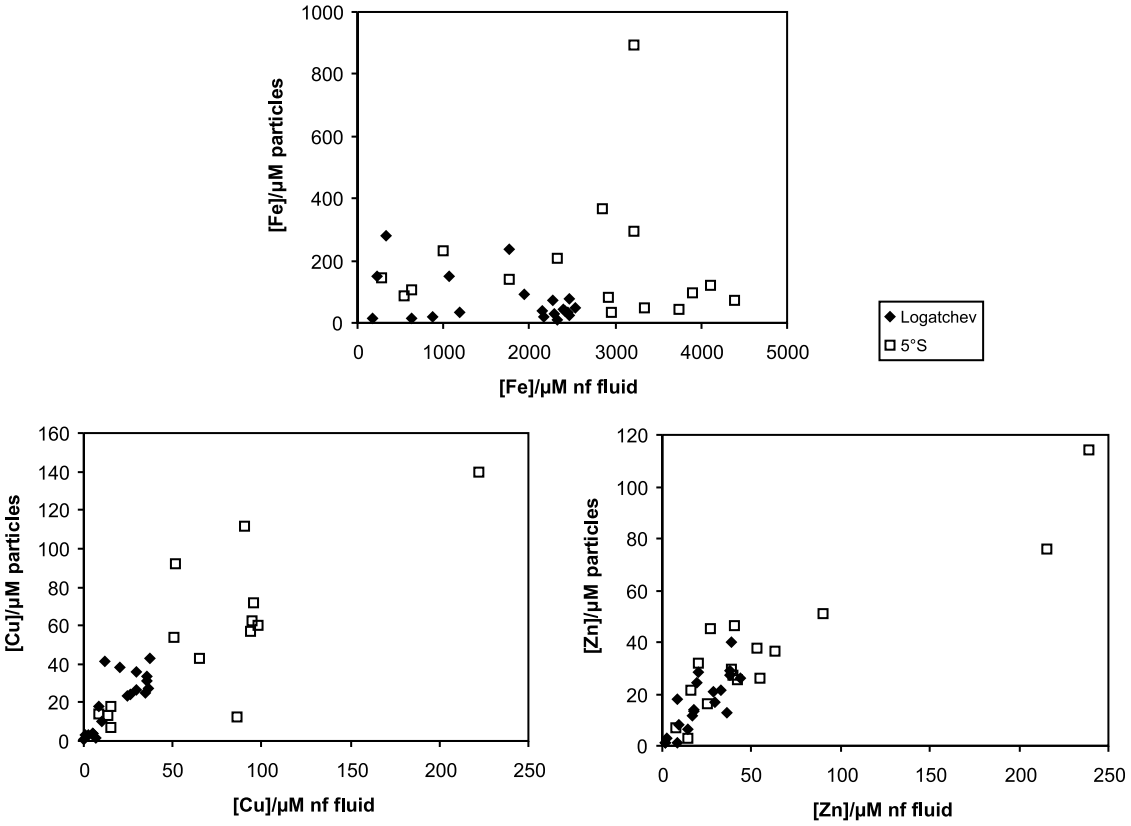

Figure 2. Correlation of Fe, Cu, Zn concentrations in the particles for Logatchev I and 5°S samples with their respective concentration in the non-filtered (nf) fluid.

[*Rempel et al.*, 2006]. The Mo content in the mixed fluid at Logatchev I can be ascribed mainly to seawater, which contains high concentrations of Mo (119 nM [*Schmidt et al.*, 2011]). The observation that Mo, which is highly immobile and precipitates as high-temperature sulphide phase [*Hannington et al.*, 1991; *Tivey et al.*, 1995; *Metz and Trefry*, 2000], is not present in vent fluids with temperatures ≤350°C, suggests that Mo is already co-precipitated with chalcopyrite during ascent [*Metz and Trefry*, 2000].

[25] Another important trace metal is Pb with an average particle concentration of ~90 nM in both areas. It shows a good correlation with Zn in the particles, which was observed before in hydrothermal vent particles [*Metz and Trefry*, 2000; *Schmidt et al.*, 2007]. Moreover it shows the best

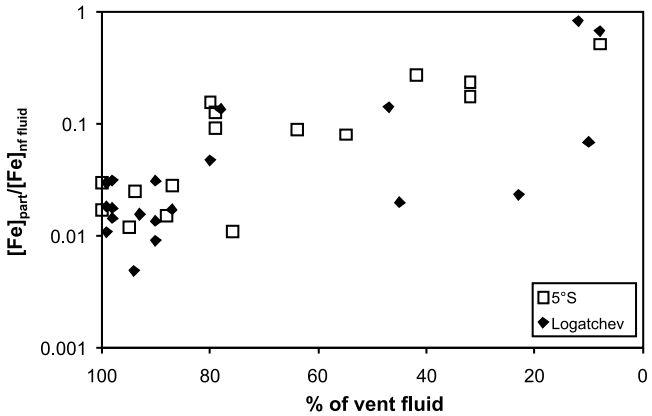

Figure 3. Plot of the fraction of Fe bound to particles versus the percentage of hydrothermal vent fluid in the sample. Nf fluid stands for not filtered fluid.

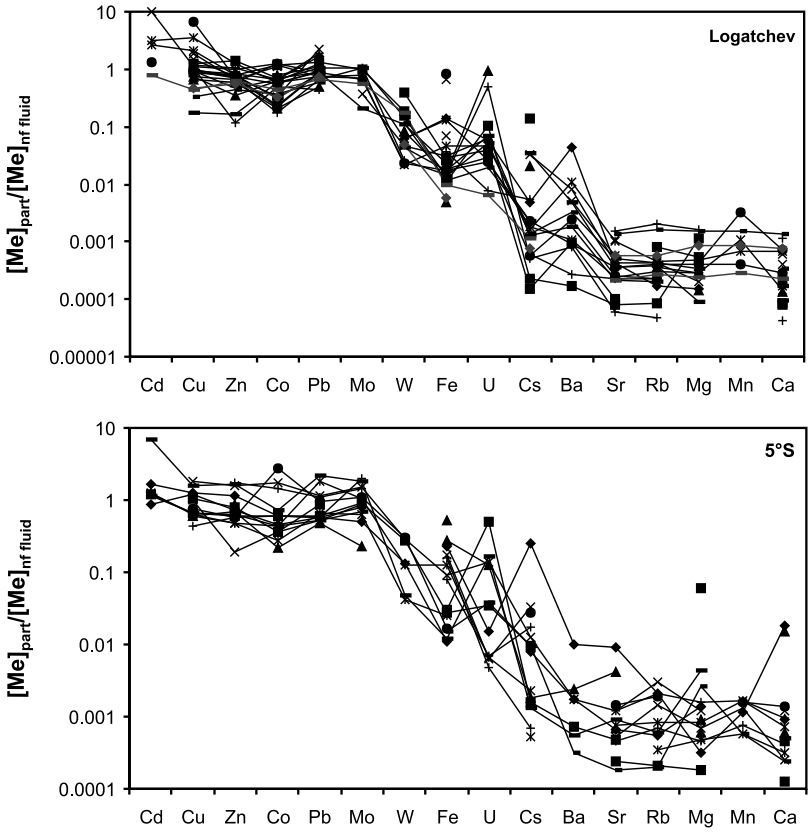

Figure 4. Fractions of metals precipitated in particles of the total concentration in the un-filtered (nf) fluids. Elements are sorted by the degree of fractionation between fluid and particles.

correlation of all elements with its concentration in the fluid (R^2 = 0.97, p = 0.93).

[26] Cadmium behaves similar to Pb, as it also correlates with Zn in the particles, indicating a close association of Cd with Zn-sulphides. This trend also was observed for near-vent plume particles and incorporation of Cd as trace component into wurtzite or sphalerite was suggested [*Trocine and Trefry*, 1988]. Concentrations of Cd are higher in 5°S particles (average 120 nM) than in Logatchev I samples (average 31 nM), which might be ascribed to slightly higher Cd concentrations in the 5°S fluids compared to the Logatchev I fluids (K. Schmidt, unpublished data, 2006, 2008; V. Klevenz, unpublished data, 2009).

[27] Although Mn is the metal with second highest concentration in the fluids, its concentration in the particles is low ranging from 0.13 to 1.3 μM, amounting to $Me_{particle}/Me_{fluid}$ ratios between 1^{-5} and 1^{-3} of the total Mn concentration in the vent fluid. It is only a trace component in sulphides, probably substituting for Zn in sphalerite [*Haymon and Kastner*, 1981; *Tivey et al.*, 1995]. A positive correlation of Mn with Zn confirms an affinity for sphalerite. Mn-oxyhydroxides do not precipitate in close proximity to the vent due to very slow oxidation of Mn^{2+} [*Haymon and Kastner*, 1981].

[28] Uranium is not contained in the pure hot end-member fluid, as mafic and ultramafic rocks do not contain significant amounts of U (0.17–1.83 ppm in basalts [*Bailey et al.*, 1993], and 0.018 ppm in primitive mantle rocks [*Gill and Williams*, 1990]) and as U is immobile under reducing conditions and removed from the fluid [*Chen et al.*, 1986]. Instead U in the particles is derived from seawater (14.3 nM [*Douville et al.*, 2002]). Its concentration in the particles is low (0.01–2.0 nM) and not correlated with fluid concentration. Sorption would be a process probably explaining its presence in the particles, as there are no U-minerals known to form in the hydrothermal fluids.

3.1.3. Alkaline and Earth Alkaline Metals (Ca, Sr, Mg, Ba, Rb, Cs)

[29] Calcium concentrations generally range from 1 to 40 μM, with two samples from 5°S falling

outside this range, 197 and 223 μM at Sisters Peak and Turtle Pits respectively, suggesting the presence of larger amounts of anhydrite that might have been incorporated from the chimney during sampling [*Schmidt et al.*, 2010]. Although Logatchev I fluids have a higher Ca concentration than the fluids at 5°S, this is not reflected by the particles. The precipitated amounts are about the same for both vent fields resulting in larger proportions of Ca being precipitated at 5°S when compared to Logatchev I. The amount of Ca being precipitated is not correlated with the fluid concentration, since only a tiny fraction of the Ca content of the vent fluids is present as anhydrite particles (<1%). This is related to its retrograde solubility at temperatures below 150°C [*Bischoff and Seyfried*, 1978]. Since its dissolution kinetics are fast (several hours until anhydrite particles are dissolved in seawater [*Feely et al.*, 1987]), most of the originally precipitated anhydrite re-dissolves in the sample bottle before filtration.

[30] Strontium concentrations range from 6 to 130 nM, with the exception of the two Ca-rich samples mentioned above that show a co-enrichment of Sr with Ca and reach 292 and 692 nM Sr, respectively. The positive correlation of Sr with Ca can be explained by the incorporation of Sr into anhydrite [*Shikazono and Holland*, 1983]. As Sr also correlates with Ca in the fluids, consequently the apparent partition coefficients of Sr and Ca are correlated with each other, both varying between 9e-4 and 10e-4. However, the two samples with exceptional high amounts of anhydrite have first, a larger Ca partition coefficient around 2e-2 and second, a Sr/Ca ratio at the lower end of the range (0.001, respectively 0.003, out of a range from 0.003–0.025). As the Sr partitioning coefficient determined by $(Sr/Ca)_{anhydrite}/(Sr/Ca)_{fluid}$ is <1 [*Teagle et al.*, 1998, and references therein], the Sr/Ca ratio of the fluid increases during fluid evolution when anhydrite precipitates [*Mills et al.*, 1998]. Moreover the Sr/Ca ratio of the hydrothermal fluid increases with increasing dilution by seawater, as seawater has a Sr/Ca ratio of 0.0087 while the end-member fluids have a Sr/Ca ratio between 0.003 and 0.004 [*Koschinsky et al.*, 2008; *Schmidt et al.*, 2011]. The lower Sr/Ca of the high anhydrite samples might therefore point to a less evolved or less diluted parent fluid.

[31] The concentration of Mg in the vent fluids is increasing with dilution by seawater, as the end-member fluids do not contain Mg at the studied vent fields. Its concentration in the particles is positively correlating with its concentration in the mixed fluids, ranging from 0.4–30 μM. One particle sample has a higher Mg concentration of 40 μM (Comfortless Cove), making up a significant part of the elements that are precipitated. Generally samples from 5°S tend to have a higher Mg content in the particles when compared to those from Logatchev I at any given Mg vent fluid concentration. Magnesium minerals likely to form in vent fluids are talc, Mg-Ca sulphates and Mg-hydroxysulphate-hydrate [*Haymon and Kastner*, 1981]. Talc also was found by EDX microprobe in 5°S particle samples.

[32] Barium is occurring in low concentrations in the particles, amounting to small fractions of the total Ba of the fluid between 1^{-5} and1^{-2}. Generally, it is more abundant at Logatchev I (up to 280 nM) than at 5°S (<20 nM). This is directly related to fluid chemistry with a Ba concentration in the end-member fluids of up to 50 μM at Logatchev I and between 5–7 μM at 5°S. Barium is usually precipitated as barite in seafloor hydrothermal systems and rare barite has been observed at Logatchev I [*Kuhn and Shipboard Scientific Party*, 2004; *Schmidt et al.*, 2007].

[33] Rubidium and Cs do not have a strong affinity for secondary minerals forming in the hydrothermal vent [*Palmer and Edmond*, 1989], and their concentrations in the particles from Logatchev I and 5°S are very low, Rb below 15 nM, and Cs mostly below 2 nM, and not correlating with fluid concentrations. Two samples with strongly elevated Cs concentrations in the particles exist, 11 and 22 nM respectively. A possible mineral known to take up Cs is chlorite [*Palmer and Edmond*, 1989], however, this mineral has not been found during our study.

3.2. Mineralogy of Vent Particles

[34] The quantitative mineralogical composition was calculated using the geochemical data (Table 2) based on stoichiometric molar S/(Cu+Fe+Zn) ratios: First, all Ca was paired with S for anhydrite ($CaSO_4$). All Cu was assumed to be related to chalcopyrite ($FeCuS_2$), taking the same amount of Fe and the double amount of S. In case there was not enough S, a CuS phase was assumed. Zinc was paired with the remaining S in a ZnS phase. If there was still S left, it was paired with the remaining Fe in FeS_2. If there was an S deficit, the excess Fe was assumed to be bound to Fe-oxides. If there was more S than Fe in the end, the S was assumed to be native S.

[35] The calculated data (Table 3) are in good agreement with the observed mineralogy of selected particle samples, examined by microprobe, EDX, and binocular microscope [*Schmidt et al.*, 2007; this study]. The mineralogy of particle samples from the Logatchev I hydrothermal field is characterized by a dominance of Cu- (chalcopyrite), Fe- (pyrite, pyrrhotite), Zn-sulphides (wurtzite, sphalerite). Some samples show noticeable amounts of anhydrite, while barite is rare. In contrast, particles filtered from gray smoke fluids at the main mound of Irina II (i. e., venting at cooler temperatures well below 300°C) are dominated by idiomorphic wurtzite and sphalerite as well as pyrrhotite. Particles sampled from the smoking crater black smoker fluids at Irina I and site B are dominated by Cu-sulphides, with minor Fe sulphides. At Quest oxidized Cu sulphides (likely covellite, as observed by binocular microscope) with minor Fe and Zn sulphides were found.

[36] Particle samples of Turtle Pits and Sisters Peak (at Comfortless Cove) at 5°S are dominated by Fe-, Cu-, and Zn- sulphides. At Turtle Pits, a few samples show appreciable amounts of native sulphur in close association with talc (Figure 5). One sample from Sisters Peak (Comfortless Cove) revealed abundant anhydrite besides sulphides.

3.3. Relationship Between Extent of Seawater Entrainment and Particle Formation

[37] There is no correlation between the hydrothermal fluid/seawater mixing ratio (based on Mg concentrations) and metal concentration in the particles (based on the sum of Fe+Cu+Zn+S in the particles). This lack of correlation also was noticed for the lower 20 m of the buoyant plume above hot springs on the East Pacific Rise near 21°N [*Mottl and McConachy*, 1990]. The authors attribute this observation to the turbulent nature of mixing between hydrothermal vent fluid and seawater in the rising plume. However, the greatest abundance of particles (>150 μmol minerals/L fluid) was observed in some fluid samples with large proportions of seawater (Figure 6). That the amount of particles present is highly variable, again, is due to the turbulence of mixing. For instance, the fact that a fluid sample with 98.7% seawater and only 1.3% contribution from vent fluid at Logatchev I has >25% of high-temperature precipitates (anhydrite and chalcopyrite) cannot be explained with in situ precipitation. It reflects turbulent transport of particles formed at high vent fluid/seawater mixing ratios into parts of the plume where the fluid is seawater-dominated. Superimposed onto the large variance in particle abundance, however, is a general trend of increasing proportions of Fe minerals with increasing mixing ratios. Apparently, the precipitation of large amounts of Fe minerals does not take place if entrainment of seawater is small (Figure 6). This observation is corroborated by the partitioning of Fe between particulate and dissolved Fe (Figure 2), which shows an increase in the proportion of particulate Fe with increasing dilution of the vent fluid by seawater. Both diagrams indicate that a proportion of >20% seawater in the mixed fluid seems to be required to form large amounts of Fe minerals in the plume.

[38] The proportions of minerals in the particles derived from mass balance calculations of chemical data of the particles (Figure 6 and Table 3) for Logatchev I samples indicate a correlation between the quantity of some minerals and the seawater/vent fluid mixing ratios. The calculated modes indicate that chalcopyrite and Zn sulphide (sphalerite and/or wurtzite) make up >80% of the precipitate in samples with <10% of seawater entrained in the sample. The proportion of Cu and Zn sulphides decreases with increasing dilution by seawater. The abundance of Fe sulphides and Fe oxides show the opposite trend; they precipitated in large quantities in samples with large amounts of seawater. Pyrite typically contributes to 20–50% of the particles in samples with >10% seawater entrained, while Fe oxides are abundant in samples with >50% seawater contribution (Figure 6). Microprobe EDX analyses of particles from samples with high proportions of hydrothermal fluid confirm the dominance of Cu sulphides over Fe sulphides [*Schmidt et al.*, 2007]. Calcium sulphate, calculated as anhydrite, occurs in variable, but generally low amounts (<25%) regardless of the extent of mixing.

[39] The particles in samples from 5°S show similar trends, although less pronounced, as those from Logatchev I with respect to the abundance of chalcopyrite, ZnS and pyrite in relation to the fraction of seawater in the mixed fluids. Due to the lower number of samples, a detailed assessment of the particle mineralogy is not possible. A striking feature of the fluids from the 5°S area is the higher total amount of precipitated particles per liter fluid in comparison to the Logatchev I fluids. In the 5°S fluids with >80% proportion of vent fluid particle concentrations range from 156 to 271 μM/L fluid (Logatchev I: 37–123 μM/L). Samples with less than 80% vent fluid contribution have dissolved

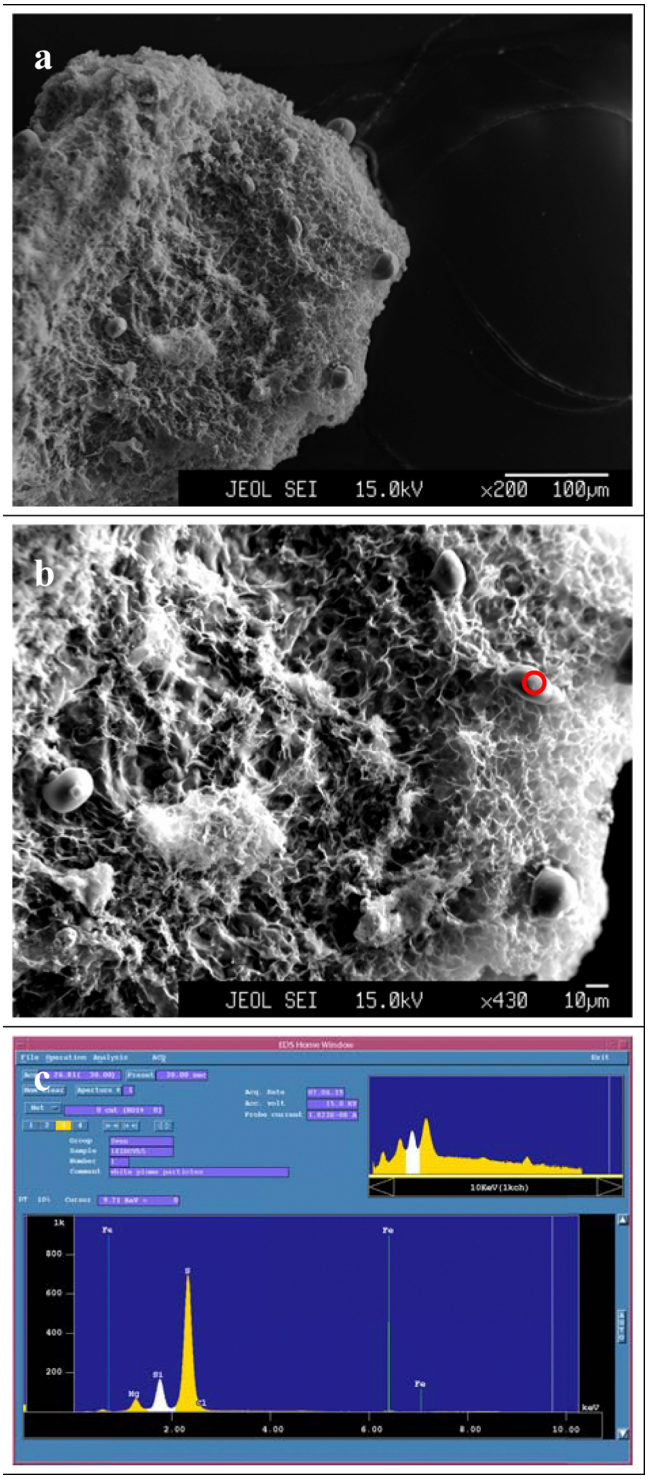

Figure 5. (a) Plume particle from Turtle Pits (sample 141ROV-B-F4) composed of Mg-Si-(Fe)-Phase (likely talc) with droplets of native sulphur. (b) Close-up showing clay-like texture of the major phase and several droplets of native sulphur. (c) EDX of sulfur-rich droplets (circle in Figure 5b). Mg, Si and Fe are from surrounding material. Particle associations of talc and native sulphur (besides common sulphides and anhydrite) were also observed in particle samples from stations 3 ROV-10 and 12 ROV-8 (Turtle Pits).

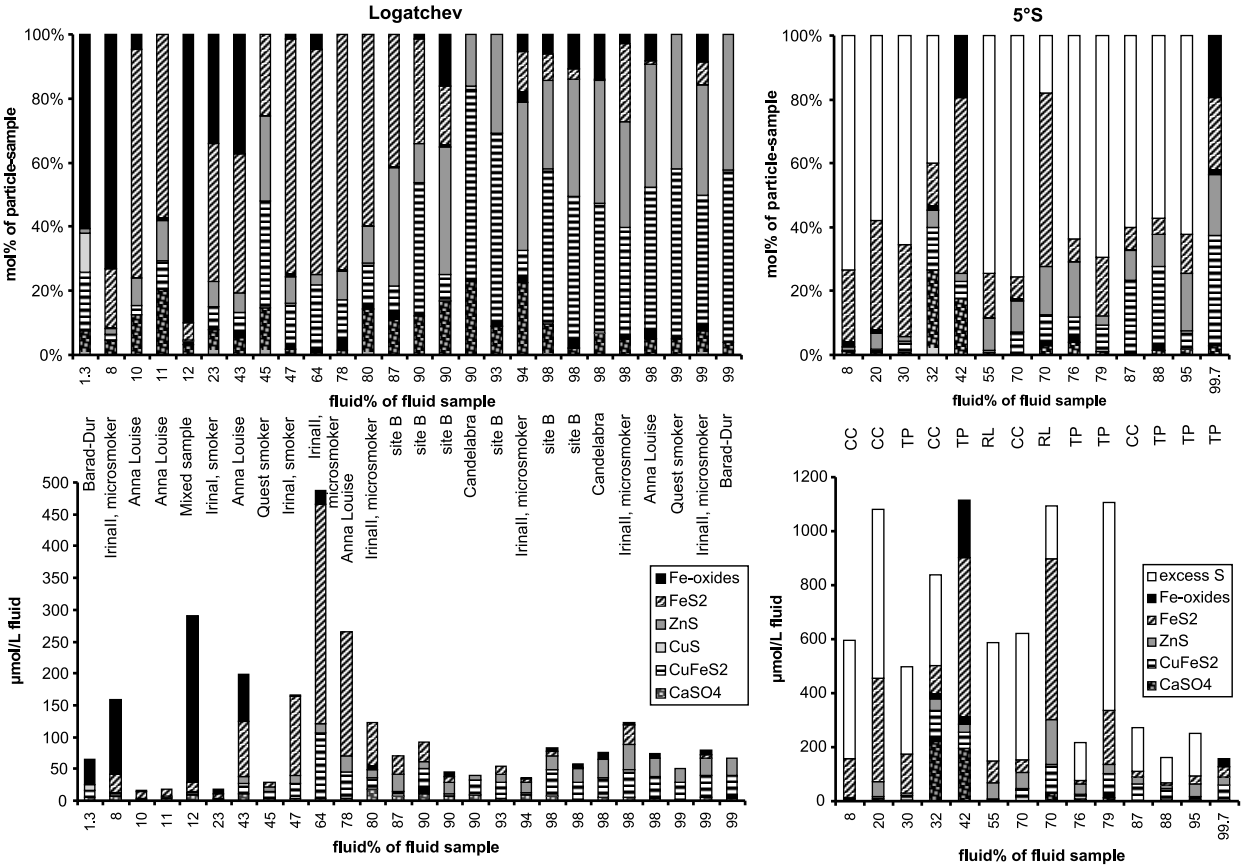

Figure 6. Calculated mineralogy of vent fluid particles (left) at Logatchev I and (right) at 5°S. (top) Mol% of the mineral in the samples. (bottom) Absolute mineral content in the fluid. CC = Comfortless Cove, TP = Turtle Pits, RL = Red Lion. Note the change in *y* axis between Logatchev I and 5°S.

particle concentrations of 586–1116 μM/L at 5°S and 16–486 μM at Logatchev I. The metal/S ratio is higher in the Logatchev I bulk particles than in the 5°S samples. The presence of elemental sulphur in most samples from 5°S predicted from mass balance calculation was confirmed by microprobe analyses. In contrast, Fe oxides (abundant in samples with large fraction of seawater from Logatchev I), are rare or absent in samples from the 5°S area. Examining relative proportions of mineral phases in the samples, the differences between the hydrothermal areas are higher percentages of Cu sulphides and Zn sulphides at Logatchev I when compared to 5°S. This is due to the large proportion of S at 5°S in most of the samples, which is between 60 and 70% of the sample composition.

[40] We propose that the pronounced differences in particle mineralogy between the Logatchev I and 5°S hydrothermal areas reflect primary differences in the end-member vent fluid composition. H_2S concentration up to 8000 μM in 5°S fluids [*Seifert and Shipboard Scientific Party*, 2009] are much greater than maximum concentrations of 2500 μM in the Logatchev I fluids [*Schmidt et al.*, 2011]. Probably more important, the Fe/H_2S ratio is <1 at 5°S, and between 1.5 and 4 at Logatchev I. These differences in fluid chemistry are reflected in the particles precipitating from the fluids. In congruence with the total amount of minerals, the amount of precipitated metals is higher at 5°S (average Fe+Cu+Zn = 300 μM, range 88–987 μM) than it is at Logatchev I (average Fe+Cu+Zn = 124 μM, range 14–589 μM). We will expand our discussion on relations between fluid chemistry and the nature of the precipitates in the next section.

[41] In summary, the particle mineralogy and solid-fluid metal partitioning show systematic trends with increasing proportion of seawater in the mixed fluids, in particular for the Logatchev I sample suite. The relative amounts of Cu sulphides in the samples (Figure 6) are greatest in the nearly un-diluted fluid, and decrease markedly with increasing dilution

Table 3. Calculated Mineral Composition (From Geochemical Data) of Particles From 5°S and Logatchev I[a]

Vent	Sample	Fluid (%)	$CaSO_4$ (μM)	$CuFeS_2$ (μM)	CuS (μM)	ZnS (μM)	FeS_2 (μM)	Fe Oxides (μM)	Native S (μM)
				5°S					
Sisters Peak	Ata 42ROV14	8	6	2		7	143		436
	Ata 42ROV11+12	*20*	7	12		56	380		626
	M68/1 20ROV5	32	223	112		46	122		336
	Ata 42ROV2−5,7	*70*	2	44		60	47		469
	M68/1 20ROV6	87	1	62		25	20		163
Turtle Pits	Ata 57ROV2,3,5	*30*	3	18		8	144		327
	Ata 46ROV7	42	197	60		27	616	216.1	
	M68/1 12ROV5	76	4	14		45	30		156
	Ata 57ROV4	79	12	92		32	202		770
	M68/1 3ROV10	88	2	43		16	8		92
	M68/1 12ROV8	95	8	18		37	15		138
	Ata 35 ROV8	99.7	5	54		30	38	30.5	
Red Lion	Ata 67ROV4+7	*55*	5	4		59	82		436
	Ata 67ROV5−7	*70*	30	108		166	594		196
				Logatchev I					
Baradur	Ata 13ROV 1	1.3	4.9	12	8.1	0.8		39.6	
	MSM04/3 275ROV5	99	2.7	36		29			
Site B	MSM10/3 313ROV12	87	7.8	7.3		26	29.2		
	Ata 30ROV3	90	11.3	39		11	30.4	1.2	
	Ata17ROV3	90	7.7	3.7		18	8.7	7.3	
	Ata 30ROV5	93	3.7	25		13	12.2		
	MSM04/3 255ROV4	98	8.0	40		23	6.9	5.1	
	MSM04/3 255ROV3	98	1.3	27		21	1.9	6.1	
Candelabra	Ata30ROV8	90	9.0	24	0.4	6.4			
	MSM04/3 255ROV17	98	5.2	31		29	0.3	10.8	
Quest smoker	Ata 24ROV11	45	4.3	10		7.9	7.5		
	MSM04/3 259ROV25	99	2.4	27		21			
Irina II microsmoker	Ata 24ROV5	8	7.2	3.1		2.6	29.5	115.7	
	MSM10/3 290ROV11	80	17.8	18		14	73.8		
	Ata 24ROV2	94	8.3	3.6		17	5.8	2.0	
	MSM04/3 253ROV9	98	6.2	43		40	29.9	3.7	
	MSM04/3 244ROV7	99	5.9	33		27	5.9	6.7	
Irina II, main structure	MSM04/3 244ROV3	64	3.1	104		15	343.8	22.3	
Irina I smoker	Ata17ROV13	23	1.4	1.2		1.3	7.5	5.9	
	MSM04/3 255ROV12	47	3.1	24		14	123.2	2.6	
Anna Louise smoker	Ata 13ROV6	10	1.9	0.5		1.3	11.1	0.7	
	Ata 13ROV9	11	3.6	1.6		2.2	10.3	0.0	
	Ata 13ROV10	43	10.4	16		12	85.8	74.2	
	MSM10/3 315ROV19	78	3.8	42		24	195.8		
	MSM04/3 275ROV7	98	3.6	35		28	0.8	6.2	
Mixed sample	Ata 30ROVA1	12	9.4	3.2		1.1	15.2	262.5	

[a]Fluid% gives the mixing grade of the fluid sample, from which the particle sample is derived. An empty space in the table means the calculated phase is not present in the sample.

of vent fluid by seawater. Likewise, the fraction of total Fe associated with precipitates increase significantly as seawater proportions in the samples go up. This type of behavior is to be explained by the strong temperature – controlled solubility of Cu sulphides (i. e. chalcopyrite), decreasing sharply between 400 and 300°C [*Seyfried and Ding*, 1995]. The reason for this sudden drop in solubility is the strong temperature control of metal complexation stability (which also depends on pH). In most submarine hydrothermal vent fluids chloride is the major ligand that complexes metals and the stability of metal-chloride complexes decreases markedly along reaction paths of decreasing temperature and increasing pH associated with vent fluid - seawater mixing [*Seyfried and Ding*, 1995]. In the Logatchev I samples Zn sulphides are also most common in samples least diluted by seawater and decrease in abundance with increasing fluid dilution. As the concentration of Zn in seafloor hydrothermal vent fluids is not known to be temperature-controlled between 400 and 200°C [*Metz and Trefry*, 2000], these particles are probably precipitated only after conductive cooling of the fluid sample on its way

from the seafloor to the ship. The solubility of sphalerite drops by an order of magnitude upon conductive cooling from 200°C to 150°C [*Seyfried and Ding*, 1995]. That Zn sulphide concentrations are highest in the least diluted samples might alternatively also be due to in situ particle loss in higher diluted samples caused by the turbulent nature of the emanating fluid. In contrast, the amounts of FeS_2 and Fe-oxides are larger at higher dilution. Fe-solubility also slightly decreases as temperatures drop, but this effect is partly counteracted by a decrease in pH due to the temperature decrease [*Seyfried and Ding*, 1995]. Although there are differences in the fluid chemistry between the three vent sites at 5°S (Cu and Fe concentrations are much higher in Turtle Pits and Comfortless Cove fluids than in Red Lion fluids), these do not affect the composition of the particle samples. Apparently, absolute concentrations of individual metals in the fluids are not as important in controlling sulphide precipitation as metal/H_2S ratios, as well as the cooling and mixing paths of the fluid.

3.4. The Model and Comparison With Measured Data

[42] Two sets of model calculations were run for each of the four vent sites (Figure 7). One model scenario (cooling) considers admixing of only 3% of seawater to the vent fluid; it predicts the minerals that should precipitate from a high-quality vent fluid sample upon cooling in the sampler. The other model (mixing) predicts mineral precipitation upon mixing in the buoyant plume. The model paths represent instantaneous fluid-solid equilibrium and do not allow minerals formed early in the cooling path to back-react at a lower temperature. These assumptions affect the results on the low temperature end, where kinetic inhibition is likely to affect fluid-solid equilibrium during precipitation. For instance, anhydrite, which is known to re-dissolve at temperatures <150°C, remains abundant throughout the reaction path. The predictive power of the thermodynamic calculations is hence diminished at the low-temperature end of the reaction paths, where kinetic processes become increasingly important [*Houghton and Seyfried*, 2010].

[43] In the Logatchev I fluid samples with an admixture of 5% or less seawater, Cu and Zn sulphides are most abundant, followed by pyrite (Figure 1). This is consistent with the model results: chalcopyrite and sphalerite are the most abundant sulphides and occur in sub-equal amounts. Pyrite is less abundant than predicted at 25°C and native sulphur is not observed at all. This mismatch is likely due to the fact that fluid-solid equilibrium did not prevail at temperatures below ~100°C. Likewise, the fact that anhydrite is much less abundant in the particles (<10%) than predicted reflects the dissolution of anhydrite, which is not anticipated in the model. The fact that dissolution was incomplete in most cases is more evidence for disequilibrium at temperatures below ~100°C where anhydrite dissolution should be complete. Models run with mineral precipitation suppressed allow us to determine possible metastable precipitates (Figure 8). This assessment of saturation states indicates that Fe oxides are super-saturated throughout most of the cooling path. Their formation in the equilibrium assemblage is hindered by the formation of Fe sulphides. However, they will form if the formation of sulphides is kinetically inhibited. Hence, it is not unexpected to find Fe oxides even in the Logatchev I samples with little seawater admixed to the vent fluid. They likely form instead of pyrite, the formation of which is known to be sluggish [e.g., *Schoonen and Barnes*, 1991]. The apparent mismatch between model and observation with respect to pyrite abundance (overpredicted by the model) and the formation of Fe oxides (not predicted by the model) can hence be explained by a simple kinetic effect.

[44] Only two of the samples from 5°S have ≥95% end-member vent fluid component and both come from the Turtle Pits vent site. One sample is characterized by the presence of native sulphur, while the other sample contains Fe-oxides. The model for admixing 3% seawater to the hypothetical end-member predicts sulphur to form, which is in agreement with our observations: Native sulphur is present in the sample containing a 5% admixture from seawater while the most undiluted sample (only 0.3% seawater admixture) does not contain native sulphur.

[45] For the particles precipitated from fluids with >5% seawater entrained during sampling, we note that the principal difference between the vent fields with respect to particle composition is the presence or absence of sulphur, which is abundant in all vents from the 5°S area, but is lacking in the samples from Logatchev I. The results of the mixing model predict sulphur to form at higher temperatures and in greater proportions in the 5°S fluids when compared to those from Logatchev I. In samples from the Sisters Peak site, sulphur is most abundant. For these fluids, the mixing model

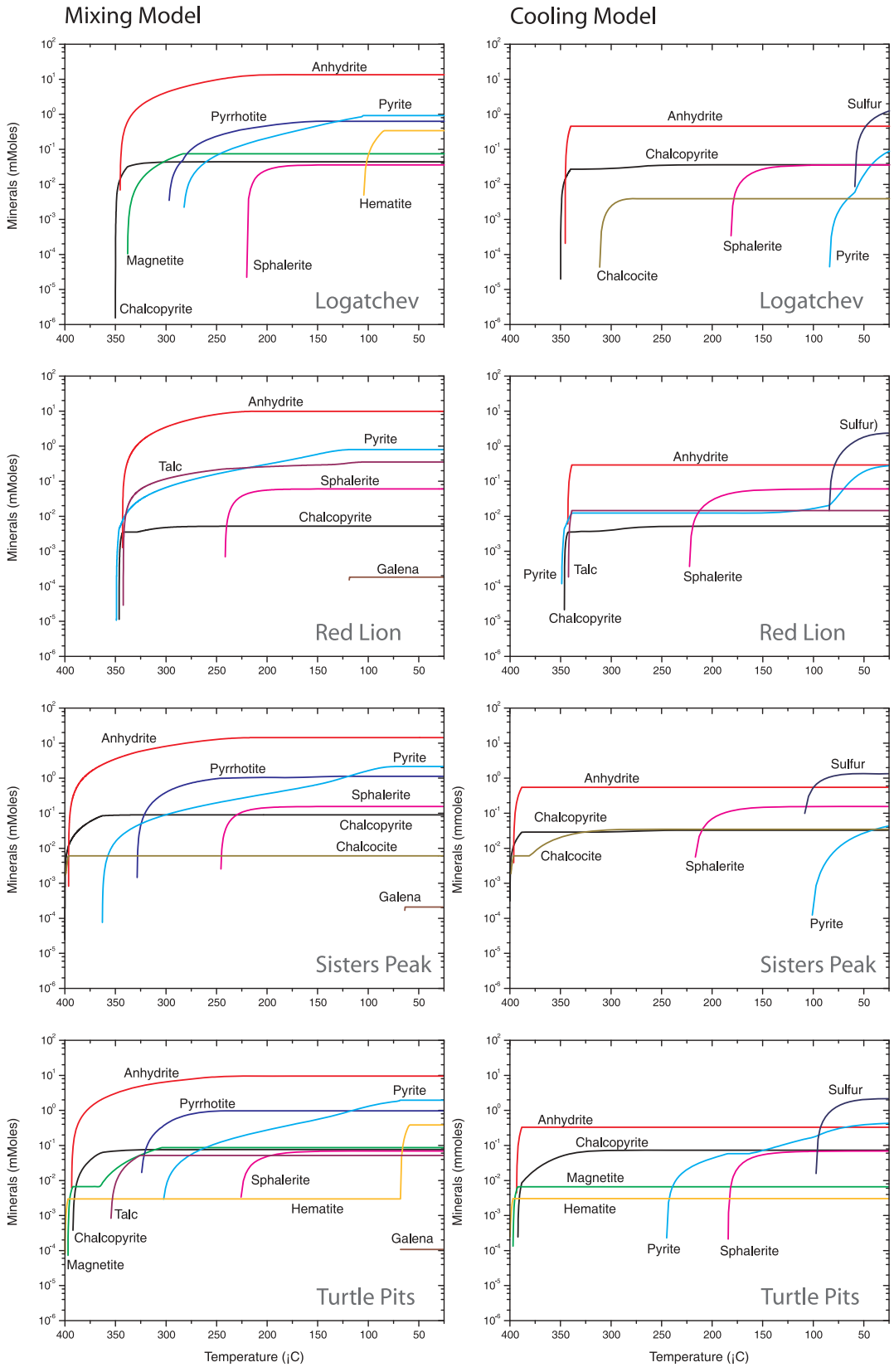

Figure 7. Results of GWB modeling (left) of mixing between hydrothermal fluid and seawater and (right) of cooling of a 97% hydrothermal fluid −3% seawater mixture. Each of the four vents (Logatchev I, Red Lion, Sisters Peak, and Turtle Pits) was considered. See text for discussion.

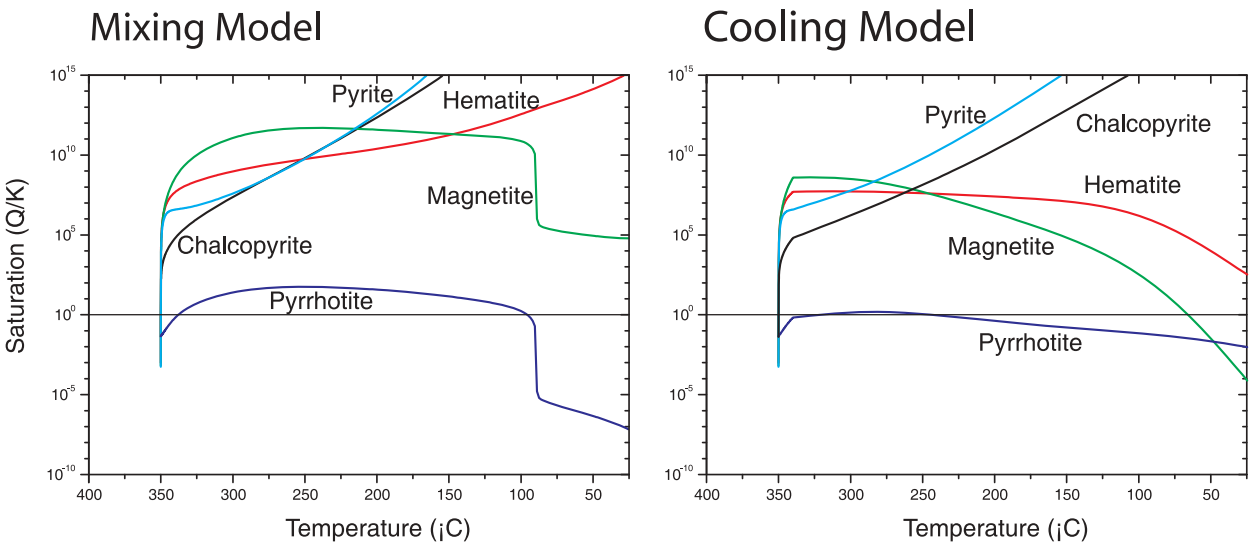

Figure 8. Saturation indices (Q/K) of Fe-bearing minerals in Logatchev I fluids along both mixing and cooling reaction paths, calculated with mineral precipitation suppressed. Note that Fe-oxides are strongly oversaturated and may hence precipitate at higher temperatures than indicated in Figure 6, if sulfide precipitation is kinetically inhibited.

predicts sulphur to begin precipitation before pyrite at temperatures >100°C, where kinetic inhibition may be small.

[46] The model results of the mixing path and the cooling path for each fluid differ in that the total amount of precipitated minerals is larger for mixing than for cooling of the respective fluid. This is in part due to a larger amount of anhydrite precipitated caused by the high SO_4 content of seawater mixing with the hydrothermal fluid. But sulphide minerals are also predicted to precipitate in larger quantities during mixing than during cooling. This is probably related to the increased pH during mixing with alkaline seawater when compared to simple conductive cooling. In comparison with the mixing model the actual particle samples presented above do contain <25% anhydrite, most likely because of the fast dissolution kinetics of anhydrite at low temperatures [*Feely et al.*, 1987].

[47] Modeling suggests a larger proportion of sulphide minerals forms during mixing when compared to fluids that undergo conductive cooling. These results are in agreement with observations in our particle samples. However, the effect of increased fluid pH and decreased sulphide mineral solubility is counteracted by the dilution of the metal concentration in the end-member vent fluid by seawater. Hence, one would expect that samples with moderate proportions of seawater admixture have highest sulphide particle abundance. This behavior is indeed indicated by a distinct enrichment in sulphide abundance in samples from Logatchev I containing between 10 and 50% admixed seawater (Figure 6). The relation between seawater dilution and sulphide abundance is less obvious in samples from 5°S. The reason for this might be that not all particles precipitating over the course of mixing are collected together with the higher diluted fluid sample, while the model sums up all minerals over the course of precipitation. This is especially important, because for the majority of minerals (anhydrite, pyrite, chalcopyrite, magnetite, hematite) precipitation occurs only during the initial mixing and cooling stage above 200°C, corresponding roughly to a 50–60% end-member hydrothermal fluid (Figure 7). Furthermore, oxidative dissolution of sulphide minerals during mixing is possible, which also reduces the amount of particles [*Dunk and Mills*, 2006]. Chalcopyrite only precipitates between 350 and 250°C, which compares well to the observation of the highest Cu concentrations in particles of near-end-member fluids, compared to more diluted fluids. In contrast, sphalerite precipitation only starts at temperatures below 200°C.

[48] Further differences between particles at 5°S and at Logatchev I are also reflected by the model: For instance, modeling predicts that particles precipitated from Logatchev I fluid should be enriched in Fe-oxides (hematite and magnetite) when compared to particles from 5°S fluids. This is in agreement with the modal calculations based on the geochemical data of the particles. The absolute amounts of Fe precipitated from the fluids differ

strongly between the model data and the measured geochemical data. The model predicts Fe to be completely precipitated, while in our particle samples only about 10% of the Fe is precipitated in the initial mixing zone. Since the major Fe mineral in the model data is pyrite, also S precipitates in larger amounts than indicated by the field data. Complete precipitation of Fe as FeS in the initial mixing zone is probably prevented by slow reaction kinetics. Moreover, it was shown that Fe is kept in solution through organic complexation in the hydrothermal plume [*Bennett et al.*, 2008]. Complete precipitation of Cu and Zn is predicted by the model, consistent with the geochemical data.

3.5. Comparison of Particle Chemistry to Metal Accumulation in Mussels

[49] One implication of a higher particle load at 5°S for the hydrothermal habitats is a higher exposure to potentially toxic metals of animals which seem to be influenced by particles from the fluids, e. g. mussels of the type *Bathymodiolus* spp. In a study by Koschinsky et al. (submitted manuscript, 2011), a general enrichment of sulphide-forming elements (Cu, Cd, Zn, Pb, Mo, and Fe) in the tissues of *Bathymodiolus* spp. might indicate the influence of mineral particles on these animals. In fact, mineral particles seem to play a larger role for metal accumulation by the mussels than dissolved metal concentrations in the fluids. Correlating with the particle samples with high anhydrite content at 5°S of this study, tissue of specimens of *Bathymodiolus* spp. collected at a diffuse venting site at 5°S was enriched in Ca and Sr compared to specimens collected at Logatchev I. A similar relationship is observed for Mo being more enriched in 5°S particle samples and in the mussel tissue obtained from 5°S specimens compared to Logatchev I and its respective particle and mussel tissue samples. Barium is more enriched in Logatchev I particle and mussel tissue samples compared to 5°S. The availability of elemental sulphur at 5°S will also have an impact on the vent fauna community, since elemental sulphur is an energy source to the vent fauna [*Ruby et al.*, 1981].

4. Conclusions

[50] Geochemical analyses of particles from variable mixtures between end-member hydrothermal fluid and seawater showed the dominance of sulphide minerals in the precipitates of the Logatchev I hydrothermal field as well as of the 5°S hydrothermal fields (Turtle Pits, Comfortless Cove, and Red Lion). A pronounced difference between the two areas is the total amount of minerals precipitated. Due to lower metal/ H_2S ratios and higher absolute H_2S concentrations in the vent fluids of 5°S, larger amounts of minerals were precipitated from the fluids at 5°S when compared to fluids from Logatchev I.

[51] It appears that absolute concentrations of individual metals in the fluids are not as important in controlling sulphide precipitation as metal/H_2S ratios, as well as the cooling and mixing paths of the fluid. The degree of mixing of the vent fluid with seawater has an influence on mineral precipitation, since larger quantities of minerals only precipitate if 20% seawater or more mix with the vent fluid. Copper sulphides only form at low mixing degrees, while Fe oxides occur in fluids with a greater proportion of seawater admixed. Modeling of the hydrothermal fluid – seawater mixing process showed some differences between the model and our geochemical data, indicating that in addition to thermodynamics other factors govern mineral precipitation in the hydrothermal mixing zone. First of all, kinetics determines if the thermodynamically favored reaction takes place. Moreover, organic molecules (which were not included in the model) have an influence on the solubility of metals through complexation. For example it is known that metals are stabilized in solution in sulphide nanoparticles by organic ligands [*Lau and Hsu-Kim*, 2008]. Only recently *Yücel et al.* [2011] reported that up to 10% of the dissolved Fe of high temperature hydrothermal fluids is in the form of pyrite nanoparticles. These are thought to sink slower than particles and to be more resistant to oxidation than dissolved Fe(II) and FeS, thereby likely increasing the amount of Fe exported to the deep ocean.

[52] This study also provides information about the amount of Fe available for Fe oxide particle formation in the plume after precipitation of Fe sulphides, which is mostly more than 90% of the fluid Fe content. Nanoparticles resistant to oxidation would however be part of this fraction, likely reducing Fe oxide formation. This has implications for particulate hydrothermal export fluxes [cf. *German et al.*, 2010] and removal fluxes from seawater due to adsorption of dissolved elements from seawater onto these particles.

[53] The correlation of particle composition in this study with the results of the study on metal accumulations in mussel tissues also highlights the

importance of hydrothermal fluid – seawater mixing processes for the geochemical characterization of vent habitats.

Acknowledgments

[54] We are grateful to captains and crews of R/V METEOR, R/V MERIAN and N/O l'Atalante and to the ROV team of the IfM-Geomar (Kiel) for excellent cooperation and support on sea. The work was supported by grants from the Special Priority Program 1144 of the German Science Foundation titled "From Mantle to Ocean: Energy-, Material- and Life-cycles at Spreading Axes." This is SPP publication 63. Constructive comments of two anonymous reviewers and the editor, which improved the quality of the manuscript, are greatly acknowledged.

References

Alexander, B. W. (2008), Trace element analyses in geological materials using low resolution inductively coupled plasma mass spectrometry (ICPMS), *Tech. Rep., 18*, Jacobs Univ., Bremen, Germany.

Bailey, E. H., A. J. Kemp, and K. V. Ragnarsdottir (1993), Determination of uranium and thorium in basalts and uranium in aqueous solution by inductively coupled plasma mass spectrometry, *J. Anal. At. Spectrom.*, *8*, 551–556, doi:10.1039/ja9930800551.

Baker, E. T., and G. J. Massoth (1986), Hydrothermal plume measurements: A regional perspective, *Science*, *234*(4779), 980–982, doi:10.1126/science.234.4779.980.

Batuev, B. N., A. G. Krotov, V. F. Markov, G. A. Cherkashev, S. G. Krasnov, and Y. D. Lisitzin (1994), Massive sulfide deposits discovered at 14°45′N, Mid-Atlantic Ridge, *BRIDGE Newsl.*, *6*, 6–10.

Bennett, S. A., E. P. Achterberg, D. P. Connelly, P. J. Statharn, G. R. Fones, and C. R. Gernian (2008), The distribution and stabilisation of dissolved Fe in deep-sea hydrothermal plumes, *Earth Planet. Sci. Lett.*, *270*, 157–167, doi:10.1016/j.epsl.2008.01.048.

Bethke, C. M. (1996), *Geochemical Reaction Modeling*, 397 pp., Oxford Univ. Press, New York.

Bethke, C. (2008), *Geochemical and Biogeochemical Reaction Modeling*, Cambridge Univ. Press, Cambridge, U. K.

Bischoff, J. L., and W. E. Seyfried (1978), Hydrothermal chemistry of seawater from 25°C to 350°C, *Am. J. Sci.*, *278*(6), 838–860, doi:10.2475/ajs.278.6.838.

Charlou, J. L., J. P. Donval, E. Douville, P. Jean-Baptiste, J. Radford-Knoery, Y. Fouquet, A. Dapoigny, and M. Stievenard (2000), Compared geochemical signatures and the evolution of Menez Gwen (37°50′N) and Lucky Strike (37°17′N) hydrothermal fluids, south of the Azores Triple Junction on the Mid-Atlantic Ridge, *Chem. Geol.*, *171*(1–2), 49–75, doi:10.1016/S0009-2541(00)00244-8.

Chen, J. H., G. J. Wasserburg, K. L. von Damm, and J. M. Edmond (1986), The U-Th-Pb systematics in hot springs on the East Pacific Rise at 21°N and Guaymas Basin, *Geochim. Cosmochim. Acta*, *50*(11), 2467–2479, doi:10.1016/0016-7037(86)90030-X.

Colaço, A., P. Bustamante, Y. Fouquet, P. M. Sarradin, and R. Serrão-Santos (2006), Bioaccumulation of Hg, Cu, and Zn in the Azores triple junction hydrothermal vent fields food web, *Chemosphere*, *65*(11), 2260–2267, doi:10.1016/j.chemosphere.2006.05.034.

Dick, J. (2008), Calculation of the relative metastabilities of proteins using the CHNOSZ software package, *Geochem. Trans.*, *9*, 10, doi:10.1186/1467-4866-9-10.

Douville, E., J. L. Charlou, E. H. Oelkers, P. Bienvenu, C. F. J. Colon, J. P. Donval, Y. Fouquet, D. Prieur, and P. Appriou (2002), The rainbow vent fluids (36°14'N, MAR): The influence of ultramafic rocks and phase separation on trace metal content in Mid-Atlantic Ridge hydrothermal fluids, *Chem. Geol.*, *184*(1–2), 37–48, doi:10.1016/S0009-2541(01)00351-5.

Drummond, S. E., Jr. (1981), Boiling and mixing of hydrothermal fluids: Chemical effects on mineral precipitation, Ph.D. thesis, Pa. State Univ., University Park.

Dunk, R., and R. A. Mills (2006), The impact of oxic alteration on plume-derived transition metals in ridge flank sediments from the East Pacific Rise, *Mar. Geol.*, *229*, 133–157, doi:10.1016/j.margeo.2006.03.007.

Dymond, J., and S. Roth (1988), Plume dispersed hydrothermal particles—A time-series record of settling flux from the Endeavour Ridge using moored sensors, *Geochim. Cosmochim. Acta*, *52*(10), 2525–2536, doi:10.1016/0016-7037(88)90310-9.

Edmond, J. M., K. L. Von Damm, R. E. Mcduff, and C. I. Measures (1982), Chemistry of hot springs on the East Pacific Rise and their effluent dispersal, *Nature*, *297*(5863), 187–191, doi:10.1038/297187a0.

Edmonds, H. N., and C. R. German (2004), Particle geochemistry in the Rainbow hydrothermal plume, Mid-Atlantic Ridge, *Geochim. Cosmochim. Acta*, *68*(4), 759–772, doi:10.1016/S0016-7037(03)00498-8.

Feely, R. A., M. Lewison, G. J. Massoth, G. Robertbaldo, J. W. Lavelle, R. H. Byrne, K. L. Von Damm, and H. C. Curl (1987), Composition and dissolution of black smoker particulates from active vents on the Juan-De-Fuca Ridge, *J. Geophys. Res.*, *92*(B11), 11,347–11,363, doi:10.1029/JB092iB11p11347.

Feely, R. A., T. L. Geiselman, E. T. Baker, G. J. Massoth, and S. R. Hammond (1990), Distribution and composition of hydrothermal plume particles from the Ashes Vent Field at Axial Volcano, Juan-De-Fuca Ridge, *J. Geophys. Res.*, *95*(B8), 12,855–12,873.

Feely, R. A., J. F. Gendron, E. T. Baker, and G. T. Lebon (1994), Hydrothermal plumes along the East Pacific Rise, 8°40′ to 11°50′N: Particle distribution and composition, *Earth Planet. Sci. Lett.*, *128*(1–2), 19–36.

Feely, R. A., E. T. Baker, G. T. Lebon, J. F. Gendron, G. J. Massoth, and C. W. Mordy (1998), Chemical variations of hydrothermal particles in the 1996 Gorda Ridge Event and chronic plumes, *Deep Sea Res., Part II*, *45*(12), 2637–2664, doi:10.1016/S0967-0645(98)00087-3.

Fouquet, Y., G. Auclair, P. Cambon, and J. Etoubleau (1988), Geological setting and mineralogical and geochemical investigations on sulfide deposits near 13°N the East Pacific Rise, *Mar. Geol.*, *84*(3–4), 145–178, doi:10.1016/0025-3227(88)90098-9.

Garbe-Schönberg, D., A. Koschinsky, V. Ratmeyer, H. Jähmlich, and U. Westernströer (2006), KIPS—A new multiport valve-based all-Teflon fluid sampling system for ROVs, *Geophys. Res. Abstr.*, *8*, 07032.

German, C. R., A. C. Campbell, and J. M. Edmond (1991), Hydrothermal scavenging at the Mid-Atlantic Ridge—Modification of trace-element dissolved fluxes, *Earth Planet. Sci. Lett.*, *107*(1), 101–114, doi:10.1016/0012-821X(91)90047-L.

German, C. R., et al. (2008), Hydrothermal activity on the southern Mid-Atlantic Ridge: Tectonically and volcanically controlled venting at 4–5°S, *Earth Planet. Sci. Lett.*, *273*(3–4), 332–344, doi:10.1016/j.epsl.2008.06.048.

German, C. R., A. M. Thurnherr, J. Radford-Knoery, J.-L. Charlou, P. Jean-Baptiste, and H. N. Edmonds (2010), Export fluxes from submarine venting to the ocean: A synthesis of results from the Rainbow hydrothermal field, 36°N MAR, *Deep Sea Res.*, *5*, 518–527.

Gill, J. B., and R. W. Williams (1990), Th isotope and U-series studies of subduction-related volcanic rocks, *Geochim. Cosmochim. Acta*, *54*, 1427–1442, doi:10.1016/0016-7037(90)90166-I.

Haase, K. M., et al. (2007), Young volcanism and related hydrothermal activity at 5°S on the slow-spreading southern Mid-Atlantic Ridge, *Geochem. Geophys. Geosyst.*, *8*, Q11002, doi:10.1029/2006GC001509.

Hannington, M., P. Herzig, S. Scott, G. Thompson, and P. Rona (1991), Comparative mineralogy and geochemistry of gold-bearing sulfide deposits on the midocean ridges, *Mar. Geol.*, *101*(1–4), 217–248, doi:10.1016/0025-3227(91)90073-D.

Haymon, R. M., and M. Kastner (1981), Hot-spring deposits on the East Pacific Rise at 21°N—Preliminary description of mineralogy and genesis, *Earth Planet. Sci. Lett.*, *53*(3), 363–381, doi:10.1016/0012-821X(81)90041-8.

Helgeson, H. C. (1969), Thermodynamics of hydrothermal systems at elevated temperatures and pressures, *Am. J. Sci.*, *267*, 729–804, doi:10.2475/ajs.267.7.729.

Houghton, J. L., and W. E. Seyfried Jr. (2010), An experimental and theoretical approach to determining linkages between geochemical variability and microbial biodiversity in seafloor hydrothermal chimneys, *Geobiology*, *8*, 457–470, doi:10.1111/j.1472-4669.2010.00255.x.

Johnson, K. S., J. J. Childress, R. R. Hessler, C. M. Sakamoto-Arnold, and C. L. Beehler (1988), Chemical and biological interactions in the Rose Garden hydrothermal vent field, Galapagos spreading center, *Deep Sea Res.*, *35*(10–11), 1723–1744, doi:10.1016/0198-0149(88)90046-5.

Johnson, J. W., E. H. Oelkers, and H. C. Helgeson (1992), SUPCRT92: A software package for calculating the standard molal thermodynamic properties of minerals, gases, aqueous species, and reactions from 1–5000 bars and 0–1000°C, *Comput. Geosci.*, *18*, 899–947, doi:10.1016/0098-3004(92)90029-Q.

Koschinsky, A., D. Garbe-Schönberg, S. Sander, K. Schmidt, H. H. Gennerich, and H. Strauss (2008), Hydrothermal venting at pressure-temperature conditions above the critical point of seawater, 5°S on the Mid-Atlantic Ridge, *Geology*, *36*(8), 615–618, doi:10.1130/G24726A.1.

Kuhn, T., and Shipboard Scientific Party (2004), The Logatchev hydrothermal field–Revisited: Preliminary results of the R/V *Meteor* cruise HYDROMAR I (M60/3), *InterRidge News*, *13*, 1–4.

Lau, B. L. T., and H. Hsu-Kim (2008), Precipitation and growth of zinc sulfide nanoparticles in the presence of thiol-containing natural organic ligands, *Environ. Sci. Technol.*, *42*(19), 7236–7241, doi:10.1021/es801360b.

Melchert, B., et al. (2008), First evidence for high-temperature off-axis venting of deep crustal/mantle heat: The Nibelungen Hydrothermal Field, Southern Mid-Atlantic Ridge, *Earth Planet. Sci. Lett.*, *275*, 61–69, doi:10.1016/j.epsl.2008.08.010.

Metz, S., and J. H. Trefry (1993), Field and laboratory studies of metal uptake and release by hydrothermal precipitates, *J. Geophys. Res.*, *98*(B6), 9661–9666, doi:10.1029/92JB00746.

Metz, S., and J. H. Trefry (2000), Chemical and mineralogical influences on concentrations of trace metals in hydrothermal fluids, *Geochim. Cosmochim. Acta*, *64*(13), 2267–2279, doi:10.1016/S0016-7037(00)00354-9.

Mills, R. A., D. A. H. Teagle, and M. K. Tivey (1998), Fluid mixing and anhydrite precipitation within the TAG mound, *Proc. Ocean Drill. Program Sci. Results*, *158*, 119–127.

Mottl, M. J., and T. F. McConachy (1990), Chemical processes in buoyant hydrothermal plumes on the East Pacific Rise near 21°N, *Geochim. Cosmochim. Acta*, *54*(7), 1911–1927, doi:10.1016/0016-7037(90)90261-I.

Palmer, M. R., and J. M. Edmond (1989), Cesium and rubidium in submarine hydrothermal fluids: Evidence for recycling of alkali elements, *Earth Planet. Sci. Lett.*, *95*, 8–14, doi:10.1016/0012-821X(89)90163-5.

Petersen, S., K. Kuhn, T. Kuhn, N. Augustin, R. Hékinian, L. Franz, and C. Borowski (2009), The geological setting of the ultramafic-hosted Logatchev I hydrothermal field (14°45′N, Mid-Atlantic Ridge) and its influence on massive sulfide formation, *Lithos*, *112*(1–2), 40–56, doi:10.1016/j.lithos.2009.02.008.

Rempel, K. U., A. A. Migdisov, and A. E. Williams-Jones (2006), The solubility and speciation of molybdenum in water vapour at elevated temperatures and pressures: Implications for ore genesis, *Geochim. Cosmochim. Acta*, *70*, 687–696, doi:10.1016/j.gca.2005.09.013.

Ruby, E. G., C. O. Wirsen, and H. W. Jannasch (1981), Chemolithotrophic sulfur-oxidizing bacteria from the Galapagos Rift hydrothermal vents, *Appl. Environ. Microbiol.*, *42*, 317–324.

Sander, S. G., and A. Koschinsky (2011), Metal flux from hydrothermal vents increased by organic complexation, *Nat. Geosci.*, *4*, 145–150, doi:10.1038/ngeo1088.

Schmidt, K. (2010), Temporal and spatial variability in the geochemistry of hydrothermal fluids and ferromanganese deposits at the Mid-Atlantic Ridge, Ph.D. thesis, 205 pp., Jacobs Univ., Bremen, Germany.

Schmidt, K., A. Koschinsky, D. Garbe-Schönberg, L. M. de Carvalho, and R. Seifert (2007), Geochemistry of hydrothermal fluids from the ultramafic-hosted Logatchev I hydrothermal field, 15°N on the Mid-Atlantic Ridge: Temporal and spatial investigation, *Chem. Geol.*, *242*(1–2), 1–21, doi:10.1016/j.chemgeo.2007.01.023.

Schmidt, K., D. Garbe-Schönberg, M. Bau, and A. Koschinsky (2010), Rare earth element distribution in >400°C hot hydrothermal fluids from 5°S, MAR: The role of anhydrite in controlling highly variable distribution patterns, *Geochim. Cosmochim. Acta*, *74*(14), 4058–4077, doi:10.1016/j.gca.2010.04.007.

Schmidt, K., D. Garbe-Schönberg, A. Koschinsky, H. Strauss, C. L. Jost, V. Klevenz, and P. Königer (2011), Fluid elemental and stable isotope composition of the Nibelungen hydrothermal field (8°18′S, Mid-Atlantic Ridge): Constraints on fluid-rock interaction in heterogeneous lithosphere, *Chem. Geol.*, *280*(1–2), 1–18, doi:10.1016/j.chemgeo.2010.07.008.

Schoonen, M. A. A., and H. L. Barnes (1991), Mechanisms of pyrite and marcasite formation from solution: III. Hydrothermal processes, *Geochim. Cosmochim. Acta*, *55*(12), 3491–3504, doi:10.1016/0016-7037(91)90050-F.

Seifert, R., and Shipboard Scientific Party (2009), Mantle to ocean on the southern Mid-Atlantic Ridge (5°S–11°S) (MAR-Süd V), cruise report, Meteor No. 78 Leg 2, Dtsch. Forschungsgemeinschaft, Bonn, Germany.

Seyfried, J. W., and K. Ding (1995), Phase equilibria in subseafloor hydrothermal systems. A review of the role of redox, temperature, pH and dissolved Cl on the chemistry of hot spring fluids at mid-ocean ridges, in *Seafloor Hydrothermal Systems: Physical, Chemical, Biologic and Geological Interactions*, *Geophys. Monogr. Ser.*, vol. 91, edited by S. E. Humphris et al., pp. 248–273, AGU, Washington, D. C.

Shikazono, N., and H. D. Holland (1983), The partitioning of strontium between anhydrite and aqueous solution from 150 to 250°C, *Econ. Geol. Monogr.*, *5*, 320–328.

Teagle, D. A. H., C. A. Jeffrey, and A. N. Halliday (1998), Tracing the chemical evolution of fluids during hydrothermal recharge: Constraints from anhydrite recovered in ODP Hole 504B, *Earth Planet. Sci. Lett.*, *155*(3–4), 167–182, doi:10.1016/S0012-821X(97)00209-4.

Tivey, M. K., S. E. Humphris, G. Thompson, M. D. Hannington, and P. A. Rona (1995), Deducing patterns of fluid-flow and mixing within the tag active hydrothermal mound using mineralogical and geochemical data, *J. Geophys. Res.*, *100*(B7), 12,527–12,555, doi:10.1029/95JB00610.

Trocine, R. P., and J. H. Trefry (1988), Distribution and chemistry of suspended particles from an active hydrothermal vent site on the Mid-Atlantic Ridge at 26°N, *Earth Planet. Sci. Lett.*, *88*(1–2), 1–15, doi:10.1016/0012-821X(88)90041-6.

Von Damm, K. L., J. M. Edmond, B. Grant, and C. I. Measures (1985), Chemistry of submarine hydrothermal solutions at 21°N, East Pacific Rise, *Geochim. Cosmochim. Acta*, *49*(11), 2197–2220, doi:10.1016/0016-7037(85)90222-4.

Wolery, T. J. (2004), Qualification of thermodynamic data for geochemical modeling of mineral-water interactions in dilute systems, Bechtel SAIC, Las Vegas, Nev.

Yücel, M., A. Gartman, C. S. Chan, and G. W. Luther III (2011), Hydrothermal vents as a kinetically stable source of iron-sulphide-bearing nanoparticles to the ocean, *Nat. Geosci.*, *4*, 367–371, doi:10.1038/ngeo1148.

Zbinden, M., N. Le Bris, F. Gaill, and P. Compere (2004), Distribution of bacteria and associated minerals in the gill chamber of the vent shrimp *Rimicaris exoculata* and related biogeochemical processes, *Mar. Ecol. Prog. Ser.*, *284*, 237–251, doi:10.3354/meps284237.